NASA TECHNICAL NOTE

NASA TN D-2480

MEASUREMENTS OF EFFLUX PATTERNS AND FLOW RATES FROM CYLINDRICAL TUBES IN FREE-MOLECULE AND SLIP FLOWS

by Harlan Cook and Edward A. Richley

Lewis Research Center
Cleveland, Ohio

NATIONAL AERONAUTICS AND SPACE ADMINISTRATION • WASHINGTON, D. C. • SEPTEMBER 1964

MEASUREMENTS OF EFFLUX PATTERNS AND FLOW RATES FROM CYLINDRICAL TUBES IN FREE-MOLECULE AND SLIP FLOWS

By Harlan Cook and Edward A. Richley

Lewis Research Center
Cleveland, Ohio

NATIONAL AERONAUTICS AND SPACE ADMINISTRATION

For sale by the Office of Technical Services, Department of Commerce,
Washington, D.C. 20230 -- Price $1.00

MEASUREMENTS OF EFFLUX PATTERNS AND FLOW RATES FROM CYLINDRICAL TUBES IN FREE-MOLECULE AND SLIP FLOWS

by Harlan Cook and Edward A. Richley

Lewis Research Center

SUMMARY

Cesium vapor efflux patterns and flow rates from cylindrical tubes varying in length to diameter ratio from 0 to 4 were experimentally determined in the free-molecule, intermediate, and slip-flow regimes. Efflux patterns in the free-molecule-flow regime were in good agreement with theory, but flow rates fell somewhat below theory for larger length to diameter ratios. Efflux patterns in the slip-flow regime showed no noticeable dependency on the tube length. Flow rates in the intermediate and slip-flow regimes agreed fairly well with theory.

With the cesium vapor used in this investigation, flux densities could readily be measured with a probe that employed the principle of contact ionization. The reliability of the probe was checked by obtaining the cosine distribution for free-molecule flow from a thin orifice.

INTRODUCTION

Efflux patterns and flow rates from ducts in free-molecule, intermediate, and slip flow are of great interest to a number of low-density-flow applications. Some examples are propellant injection ducts for electric thrustors, vacuum systems, and vacuum deposition equipment. Some theoretical analyses of efflux patterns and flow rates have been made for molecular flow, but the complexities of intermediate and slip flows have prevented rigorous analysis in these flow regimes. Experimental measurements of efflux patterns are also lacking.

Efflux patterns and flow rates for molecular flow from cylindrical tubes have been calculated (ref. 1) by assuming that the mean free path λ of the gas was not only greater than the diameter of the tube, but also greater than its length L, that is, that free-molecule flow existed throughout the tube. Clausing's approximate equation (ref. 2) was used for the particle arrival-rate distribution along the walls. These arrival-rate profiles vary by only a few percent from more exact values (ref. 3) calculated by a numerical solution

of the exact integral equation. One of the objectives of the present investigation was to verify experimentally the calculations of reference 1.

The present investigation also includes efflux patterns and flow rates from various cylindrical tubes under conditions of intermediate flow ($\lambda \approx L$) and slip flow ($\lambda < L$). The cylindrical tube length to diameter ratios were varied from 0 to 4. Cesium vapor was used since flux densities could readily be measured with a probe that employed the principle of contact ionization.

THEORY

The flow of rarefied gases can be divided into three regimes; free-molecule, intermediate, and slip flows. The free-molecule-flow regime is that for which λ, the mean free path, is large compared with a characteristic dimension of the boundary geometry, so that collisions with the walls are much more likely than collisions between particles. As the mean free path of the gas becomes comparable to the characteristic dimension, the flow passes through an intermediate regime and approaches slip flow. Slip flow differs from continuum flow in that the gas immediately adjacent to the wall of the tube appears to possess a finite velocity (i.e., a slip velocity).

The dimensionless ratio of the mean free path to the characteristic dimensions of a duct is denoted as the Knudsen number and is a useful parameter for establishing bounds that identify the various flow regimes. Present experimental evidence (ref. 4) indicates that the limits for the slip-flow regime in terms of the Knudsen number K are about $0.015 < K < 0.15$, while the limits for the intermediate-flow regime are about $0.15 < K < 5.0$. If the gas flow has a Knudsen number greater than about 5, the flow is free molecular.

Free-Molecule-Flow Theory for Thin Orifices

Knudsen (ref. 5) showed experimentally and theoretically that, in the free-molecule-flow regime, the differential molecular flow rate $d\dot{n}$ defined as the number of particles flowing into the differential solid angle $d\Omega$ making an angle θ with the outward normal from the flow area A_H is given as

$$d\dot{n}(\theta) = \frac{d\Omega}{4\pi} \sigma \bar{v} A_H \cos \theta \tag{1}$$

where σ is the molecular number density, $\bar{v}$ is the average molecular velocity, and A_H is the area of the source of flow. (All symbols are defined in appendix A.) Equation (1) is valid for the far field, where the dimensions of the flow area A_H are very small compared with the distance from that area. From equation (1), it is evident that

$$\frac{d\dot{n}(\theta)}{d\dot{n}(\theta = 0)} = \cos \theta \tag{2}$$

This cosine distribution of particles coming from a finite circular orifice will become distorted in the near field where the size of the orifice

becomes of the same order of magnitude as the distance away from the orifice and the flow no longer behaves as a point source. In appendix B, a calculation is made to determine the limit between the far and near field by considering each differential area of a thin circular orifice as a small flow area obeying Knudsen's cosine distribution law. The differential contributions from the orifice that arrive at a small area A_P ($\ll A_H$) were summed at an arbitrary point (R, θ). If the differential area of the hole is $a\ da\ d\alpha$ (see sketch (a)), Knudsen's equation for a thin circular orifice (as derived in appendix B) becomes

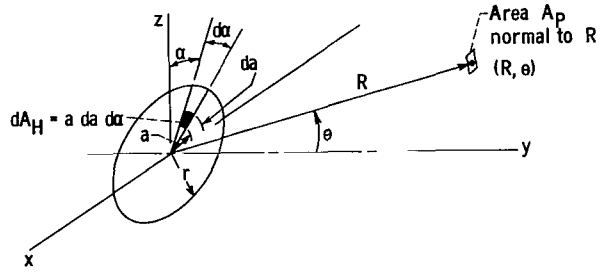

(a)

$$\dot{n}_P(\theta) = \frac{A_P \sigma \bar{v} \cos\theta}{4\pi} \left(\frac{r}{R}\right)^2 \int_{\pi/2}^{3\pi/2} \frac{d\alpha}{\left[1 + \left(\frac{r}{R}\right)^2 - 2\frac{r}{R}\sin\theta\sin\alpha\right]} \tag{3}$$

Numerical integration of equation (3) was carried out for a range of the ratio of orifice radius to distance of test point from orifice center, r/R, and these results are shown in figure 1 along with a curve of the cosine distribution given by equation (2). For $r/R \leq 0.1$, the effect of finite orifice size becomes less than 2 percent and $r/R < 0.1$ may be considered the far field. The value of r/R used in the experimental work herein was less than 0.03 so that, in this respect, the thin orifice could be considered a point source of particles obeying equation (1).

Free-Molecule Flow in Far Field of Finite Length Orifices

The distortion in the cosine distribution caused by increasing the orifice thickness from zero to some finite value was analytically investigated by Clausing (ref. 2), who added a correction factor $T(\theta)$ to equation (1) to take into account the length of the tube. Equation (1) then takes the form

$$d\dot{n}(\theta) = \frac{d\Omega}{4\pi} A_H \sigma \bar{v} \cos\theta\, T(\theta) \tag{4}$$

where $T(\theta)$ is the added correction factor. It is a function of θ varying from unity at $\theta = 0$ to less than unity as θ increases to 90°. The angular dependency of equation (4) takes the form

$$\frac{d\dot{n}(\theta)}{d\dot{n}(\theta = 0)} = \cos\theta\, T(\theta) \tag{5}$$

Clausing calculated values of $T(\theta)$ for a tube length to diameter ratio of unity; these calculations were extended for length to diameter ratios of 0.5, 1, 2, and 5 (ref. 1). In these calculations, the mean free path of the gas is assumed to be greater than the diameter and length of the tubes.

Molecular Flow Rates

Free-molecule-flow rates. - The free-molecule-flow rate through a tube may be obtained by integrating equation (4) over the total solid angle downstream of the tube. Equation (4) becomes

$$\dot{n} = \frac{A_H \sigma \bar{v}}{2} \int_0^{\pi/2} T(\theta) \cos\theta \sin\theta \, d\theta \tag{6}$$

In reference 6 the free-molecule-flow rate through a circular tube is given as

$$\dot{n} = \frac{\sigma \bar{v} A_H K_a}{4} \tag{7}$$

where K_a is the Clausing factor that corrects for the length of the tube. Equating equations (6) and (7) and solving for K_a give

$$K_a = 2 \int_0^{\pi/2} T(\theta) \cos\theta \sin\theta \, d\theta \tag{8}$$

Slip-flow rates. - Flow rates for the intermediate and slip-flow regimes are not as well defined as those for the free-molecule-flow regime. There are three equations: Knudsen's empirical equation, Maxwell's equation, and an equation based on a derivation given in reference 7. Each equation gives a different numerical value for flow rate.

Knudsen's empirical equation for the intermediate-flow regime assumes that the total molecular flow rate is merely the summation of laminar viscous flow and Knudsen flow, so that for a tube (ref. 6)

$$\dot{n} = \frac{\pi D^4 \bar{\rho} \, \Delta P}{128 \, \mu L m} \left(1 + z \, \frac{8L}{D^2} \, K_a \, \frac{\bar{v} \mu m}{\bar{\rho} k T} \right) \tag{9}$$

where ΔP is the pressure drop through the tube and z is an empirical coefficient ranging in value from about 0.8 to 1.0. In this report z has been assumed equal to unity. The Chapman-Enskog equation for viscosity is (ref. 6)

$$\mu = 0.499 \, \rho \bar{v} \lambda \tag{10}$$

where λ is the mean free path of the gas molecule:

$$\lambda = \frac{kT}{\sqrt{2}\ \pi P (d_m)^2} \tag{11}$$

Herein, the molecular diameter d_m was taken as 5.4×10^{-8} centimeter for cesium. Substituting equation (10) for viscosity into equation (9) yields

$$\dot{n} = \frac{\pi D^4\ \Delta P}{63.9\ m\bar{v}\bar{\lambda}L}\left(1 + \frac{3.99\ LK_a\bar{v}^2 m\bar{\lambda}}{D^2 kT}\right) \tag{12}$$

Maxwell's equation (ref. 8) for slip flow is given as

$$\dot{n} = \frac{\pi D^4\ \Delta P}{63.9\ m\bar{v}\bar{\lambda}L}\left[1 + 7.984\left(\frac{2}{f} - 1\right)\frac{\bar{\lambda}}{D}\right] \tag{13}$$

where f is the fraction of molecules presumed to be diffusely reflected from the walls.

An equation for the flow rate in the slip-flow regime which assumes that all molecules are diffusely reflected is given in reference 7. This relation, modified by the use of Chapman-Enskog viscosity (eq. (10)), is

$$\dot{n} = \frac{\pi D^4\ \Delta P}{63.9\ m\bar{v}\bar{\lambda}L}\left(1 + 10.63\ \frac{\bar{\lambda}}{D}\right) \tag{14}$$

APPARATUS

The vacuum facility used for this investigation had a stainless-steel chamber 9 inches in diameter and 24 inches high. The lower half of the chamber was cooled with water to a temperature of 50° F. The top of the test chamber was covered with a glass plate for visual observation. The vacuum system was equipped with a 6-inch oil-diffusion pump and a liquid nitrogen pump baffle. The pressure in the test chamber was maintained at 10^{-5} torr during the tests.

Cesium Vaporizer

The cesium vaporizer on which the test orifices and tubes were mounted is shown in figure 2. The body of the vaporizer was constructed of 1/16-inch-thick stainless steel with 1/4-inch flanges. The vaporizer was resistance-heated with two heating coils, one on the face flange and the other wound around the main body. The desired temperature was maintained in the vaporizer by adjusting the heater currents according to the temperature measurements of the two iron-constantan thermocouples. One thermocouple was placed on the back of the vaporizer to control the heater wound around the main body of the vaporizer, the other was placed on the face flange to control that heater. The temperature of the vaporizer was varied from 260° to about 500° F.

The orifice plates were made of copper to give good heat transfer to the walls of the cylindrical tubes. The cylindrical tubes used in this experiment were 0.125 inch in diameter and varied in length L from about 0 to 0.5 inch (L = 0.003, 0.0625, 0.125, 0.25, 0.375, and 0.5 in. giving ratios of length to diameter of 0.024, 0.5, 1, 2, 3, and 4).

A glass capsule containing approximately 2.5 grams of cesium was placed in the bottom of the vaporizer. The capsule was broken by the force from the electrically actuated solenoid that was transmitted to the sharp chisel attached to the bellows shown in figure 2. A small solenoid (see fig. 2(b)) was used to operate a shutter across the orifice opening to prevent the flow of cesium from the vaporizer into the probe when data were not being taken.

Neutral Cesium Probe

The neutral cesium probe and electrical circuit are shown in figures 2 and 3. The probe consisted of a 0.002- by 0.015- by 0.375-inch tungsten ribbon that was spot-welded between two 0.010-inch-diameter platinum wires. The wires were supported by two filament holders, which in turn were held in place and electrically insulated from the probe shell by a boron nitride base. The probe shell was double walled and cooled by liquid nitrogen. The principle of contact ionization (ref. 9) was utilized to obtain measurements of the cesium vapor flux density from the vaporizer. Neutral cesium atoms entering the probe through the opening in the shell came into contact with the tungsten ribbon, which was resistance-heated to about 2800° F. The tungsten ribbon was maintained at a potential of 135 volts positive with respect to ground, the outer shell being at ground potential. Cesium ions thus formed on the ribbon were collected on the outer shell. Liquid nitrogen cooling of the collector served to keep the background pressure of neutral cesium vapor at a minimum. Batteries were used in both the heating and the ion-current-monitoring circuits. The contact-ionization properties of cesium vapor on tungsten makes it an ideal gas for measuring neutral molecular efflux patterns with the probe described. Since cesium is singly ionized upon contact with tungsten, the resulting ion current is equivalent to the neutral flux intercepted by the tungsten filament. The ion current was measured by a micromicroammeter, which had an output signal proportional to the deflection of the meter.

The vaporizer was mounted in the test facility so it could be rotated horizontally about a vertical axis passing through the face of the orifice plate and bisecting the orifice opening (see fig. 2). The probe was mounted on a movable horizontal rod that could be adjusted to locate the tungsten ribbon from 2.45 to 3.45 inches away from the end of the orifice plate on the vaporizer. The vertical position of the probe was adjusted so that the axis of the orifice tube and the axis of the inlet hole into the neutral cesium probe were in the same horizontal plane.

The angular position of the vaporizer was related to an electrical signal by means of a linear potentiometer. The position signal and the probe output signal (which was proportional to the deflection of the micromicroammeter) were fed into an x-y recorder, and ion current was plotted as a function of angular

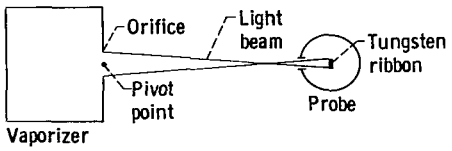

(b)

position of the probe with respect to the orifice axis.

Experimental Procedure

In operation, the probe was carefully lined up with the orifice so that the entire width of the filament was exposed to the cesium flowing from the orifice (see sketch (b)). This alinement was checked by heating the tungsten strip white hot and observing the light beam cast through the hole in the probe shell and onto the orifice plate. If the orifice was completely illuminated by this light beam for all angular positions of the vaporizer, the probe was alined satisfactorily.

A typical run consisted of first washing all metal parts of the vaporizer and probe with chromic acid. The surface of the boron nitride insulator of the probe was lightly sanded to remove any contamination. A cesium capsule was placed in the vaporizer, and the probe and vaporizer were assembled and mounted in the test facility. The facility was evacuated to a pressure of about 15 torr for approximately 15 hours to facilitate outgassing. Then the test chamber was pumped down to about 10^{-5} torr and the filament alinement was checked. The vaporizer was heated to 260° F for several hours for final outgassing. The instrumentation was checked out and the cesium capsule was broken.

Two sets of current readings as a function of the angular position were taken for each vaporizer temperature setting. One set was taken at a distance of 2.45 inches and the other at a distance of 3.45 inches away from the orifice. The vaporizer temperature was reset in intervals of 20° or 30° F and additional data taken at each setting. The maximum vaporizer temperature at which data were taken was 500° F. At this temperature the mean free path of cesium atoms was a few hundredths of an inch. The vaporizer temperature response was good, and little time was required for the system to reach steady state. The average time for a test run over the full range of vaporizer temperature settings was about 1/2 hour.

The data consisted of continuous traces of the ion current as a function of the angular position of the probe relative to the orifice. The angular position was varied from 90° (i.e., the probe parallel to the plane of the orifice) to 10° past the axis of the orifice. These data were then processed into tabular form with the ion current readings listed at angular intervals of 5°. An example of these data is given in table I. The current readings at 90° were considered to be entirely background current and were subtracted from current readings at each angular position. The tabulated current readings were normalized to the maximum current readings (probe on orifice axis) to obtain a ratio of currents that ranged from 1 to 0 (see table I). These current ratios represent the relative flux densities for the given angular positions.

The basic accuracy of the apparatus was verified by comparing efflux patterns from a thin orifice ($L/D \approx 0$) with the theoretical cosine distribution

as predicted by Knudsen (ref. 5). These results are shown in figure 4 (from table I) and it is seen that agreement is very good.

It is noted in figure 4 that the data were taken at a Knudsen number of 9.5. For this and all subsequent figures, the indicated Knudsen number was based on an average mean free path of $\bar{\lambda} = 2\lambda$, where λ is given by equation (11). Since the vapor pressure of cesium at the lowest operating temperature is about 3 orders of magnitude higher than the facility background pressure, the calculation is consistent with the assumption that the vapor pressure equals the pressure drop in equations (12) to (14) and that average values required in those equations are based on an average pressure equal to one-half the vapor pressure.

RESULTS AND DISCUSSION

Efflux Patterns

One of the objects of this investigation was to verify experimentally the calculations of reference 1. Figure 5 compares the experimental and theoretical efflux patterns for free-molecule flow (Knudsen number, 9.5) of cesium vapor from cylindrical tubes with length to diameter ratios of 0.5, 1, 2, 3, and 4. A dashed line is faired through the data points. The solid line represents the calculations of reference 1. The efflux patterns predicted in reference 1 are all more directed than those measured experimentally. A comparison of successive figures (i.e., L/D increasing) indicates that the flow becomes more directed as the tube length to diameter ratio increases. Overall agreement between experimental and theoretical flux patterns in figure 5 is fairly good, with the largest differences occurring for a length to diameter ratio of 4. Calculations show that the probe sampling area was sufficiently small to introduce no appreciable error, and, as described earlier, calculations also verified that the probe measurements were in the far field. Thus, the reason for the differences is not apparent but may be due to incomplete attainment in the experiment of the assumptions in the theoretical analysis.

The second object of the experiment was to study the efflux patterns in the near free-molecule-flow regime, that is, the intermediate and slip-flow regimes where the length of the mean free path is of the same order of magnitude or less than the diameter of the tube (i.e., $0.015 \leq K \leq 5$). The experimental values of $T(\theta)\cos\theta\left[\text{i.e., } \frac{I(\theta)}{I(\theta = 0)}\right]$ for the various tubes and for values of angular probe position of 15°, 30°, 45°, 60°, and 75° over a range of Knudsen numbers are given in figure 6. As before, dashed lines are faired through the data for the various angular positions. The three flow regimes are indicated and their limits are as defined earlier in this report. The solid lines in the left portion of figure 6 are theoretical values of $T(\theta)\cos\theta$ for the various tubes as the Knudsen number becomes large. The dashed lines shown for the five angles indicate that, except for length to diameter ratios of 0.024 and 0.5, the experimentally determined function is generally larger than the theoretical but is a decreasing function of Knudsen number near 9.5.

Thus, closer agreement between experiment and theory would be expected at larger values of Knudsen number.

The intermediate region is characterized in figures 6(c) to (f) by $T(\theta)\cos\theta$ increasing (as the Knudsen number decreases) from some fairly constant values in the free-molecule-flow regime to some higher value in the slip-flow regime. As mentioned previously, no known theoretical distributions were available for comparison with the slip-flow distributions.

It is interesting to note that, as the length to diameter ratio increases, a Knudsen number based on the tube length, instead of diameter, tends to approach slip-flow values even though the value based on diameter is still large. For example, for $K = \overline{\lambda}/D = 5$, since all tubes were 0.125 inch in diameter, the average mean free path of the cesium vapor is 0.625 inch. In figures 6(c) to (f), if the tube length were used as the characteristic dimension, the Knudsen number values would have been

Figure 6	Tube length, L, in.	Knudsen number based on tube length, λ/L
(c)	0.125	5
(d)	.250	2.5
(e)	.375	1.67
(f)	.500	1.25

Replotting figures 6(c) to (f) on this basis would result in an increasing shift of the data to the right.

Figure 7 shows the averaged experimental efflux patterns for cylindrical tubes of various length to diameter ratios for the free-molecule-flow regime ($K = 9.5$), intermediate-flow regime ($K \cong 1.9$), and the slip-flow regime ($K \cong 0.12$). Figure 7(a) for free-molecule flow shows that the efflux pattern becomes more directed as the length to diameter increases. This would be expected since the length of the tube acts as a collimator for the flow of the vapor from the vaporizer. This trend in the efflux pattern with variations of length to diameter ratio is in agreement with reference 1. Figure 7(b) for the intermediate-flow regime ($K \cong 1.9$) shows that, as the length to diameter ratio goes from about 0 to 2, the flow becomes more directed; the distribution, however, is relatively insensitive to changes in length to diameter ratio when it is greater than 2. Finally, the efflux patterns in figure 7(c) (slip flow) show no dependency on the length to diameter ratio.

Compared in figure 8 are the experimental efflux patterns for free-molecule flow ($K = 9.5$) and those for slip flow (K between 0.08 and 0.13 for each of the L/D ratios investigated). The curves are again faired in through the data points. Figure 8(a) for a length to diameter ratio near zero shows that the efflux pattern is more directed for the thin orifice in the slip-flow regime than in the free-molecule-flow regime. The efflux patterns for the two regimes are almost the same for a length to diameter ratio of 1/2

(fig. 8(b)). However, figures 8(c) to (f) for length to diameter ratios ranging from 1 to 4 show that the efflux patterns are less directed in the slip-flow regime than in the free-molecule-flow regime.

A less-directed character in the slip-flow regime, relative to the free-molecule regime, would be expected due to the spreading effect of the more numerous collisions between particles. Consequently, no explanation is available for the higher collimation attained with slip flow for a length to diameter ratio near zero. In the absence of an adequate theory for efflux patterns in the slip-flow regime, no conclusion can be reached.

Experimental Clausing Factors

In equation (8), the quantity $T(\theta)\cos\theta$ may be set equal to $\frac{I(\theta)}{I(\theta = 0)}$, the ratio of probe ion currents. Equation (8) then becomes

$$(K_a)_{exp} = 2\int_0^{\pi/2} \frac{I(\theta)}{I(\theta = 0)} \sin\theta \, d\theta \tag{15}$$

This integration was carried out by applying Simpson's rule for integration of the data for a Knudsen number of 9.5 for the various length to diameter ratios, and the results are given in figure 9. The solid curve represents the theoretical values of the Clausing factor given in reference 6. The agreement between experiment and theory is very good for length to diameter ratios near zero and at 1 and 2, while the experimentally determined values are higher than the theoretical values for 0.5, 3, and 4. Numerical integration of the data was employed to make these comparisons so that some variations would be expected.

Molecular Flow Rates

Since the molecular flux density is directly proportional to the ion current measured by the probe, the molecular flow rate can be calculated by integrating the probe current per unit area over a hemisphere of radius R and dividing by the ionic charge. The variation of flow rate with Knudsen number for the various tube length to diameter ratios is shown in figure 10. Also shown are the various theoretical curves as expressed by equation (7) for free-molecule flow, equation (12) for intermediate flow, and equations (13) and (14) for slip flow. The data of figure 10 cover 2 to 3 orders of magnitude, and the theoretical curves have been extended beyond their expected ranges of validity so that trends may be easily identified.

Varying degrees of agreement between the data and theoretical curves can be seen in figure 10. For example, the data of figure 10(a) compare well with the molecular-flow curve of equation (7), even at smaller values of Knudsen number ($K < 5.0$); however, as the tube length to diameter ratio increases (figs. 10(b) to (f)) agreement is not as good, particularly at high Knudsen numbers ($K > 5.0$). On the other hand, the data come into better agreement with the slip-flow equations as the length to diameter ratio increases. Since the

various theoretical equations themselves show a considerable spread over the "extended" ranges, absolute accuracy comparisons would not be meaningful. At best it can be said that most of the data of figure 10 fall near or within the bounds given by the various theoretical curves. The Clausing factors determined with equation (15) and shown in figure 9 depend only on the flux distribution and not on the magnitude of the flux; thus, although some free-molecule-flow rates fall below the theoretical curves (e.g., fig. 10(f)), at the same time nearly correct values of Clausing factors were determined.

Of the various experimental errors that might affect the flow-rate results, one of the most significant was the possible variation in effective probe filament area from run to run due to variations in filament width and/or alinement. This error could have been as much as 20 percent. Another possible source of error was the measurement of vaporizer temperature. A close check on this was made by installing several additional thermocouples, heating the vaporizer, then comparing the additional thermocouple readings with those used in the experiment. In all cases, the temperature readings of the extra thermocouples were at least equal to the readings of the thermocouples used during the tests, which confirmed that the ones used in the experiment were recording the lowest temperature in the vaporizer.

The cesium vapor pressure in the vaporizer may have been lower than values given on the vapor pressure curve of reference 10 for various reasons. If this occurred, the actual Knudsen number would be larger, resulting in a shift of data to the left in figure 10. Contamination of the liquid cesium is one possible cause of lowered vapor pressure in some of the runs. Knudsen (ref. 5) experienced trouble of this kind in his work with mercury. In general, the effect would be more pronounced at lower temperatures (i.e., large Knudsen numbers). Every effort was made to minimize the problem in the experiment reported herein; however, if the vapor pressure was reduced as a result of contamination the flow rates would be lower than those predicted by theory and actual Knudsen numbers would be greater. This combination might easily account for some of the difference between experimental and theoretical flow rates, particularly in the free-molecule-flow regime.

CONCLUSIONS

Measured distribution patterns for free-molecule flow were compared with the theoretical patterns predicted for large Knudsen numbers, and were in good agreement for length to diameter ratios of 0.5, 1, 2, and in fair agreement for 3 and 4.

Efflux patterns in the slip-flow regime showed no consistent dependency on the length of the tube and yielded a pattern somewhat more directed than the cosine distribution but less directed than the free-molecule flow distribution for cylindrical tubes having length to diameter ratios greater than 1. An increased number of intermolecular collisions within the tube for the slip-flow regime appear to explain the less-directed efflux at length to diameter ratios greater than 1.

Measured values of the Clausing factor for free-molecule flow were in close agreement with those given by Dushman. In general, molecular flow rates of cesium vapor through the tubes were either equal to or less than those predicted by kinetic theory for Knudsen numbers greater than about 0.8. Differences were attributed primarily to a lower actual vapor pressure than that predicted by the Taylor-Langmuir vapor pressure curve for pure cesium. Contamination of the cesium may have reduced the vapor pressure and thus the flow rates.

Lewis Research Center
National Aeronautics and Space Administration
Cleveland, Ohio, May 29, 1964

APPENDIX A

SYMBOLS

A_H	cross-sectional area of orifice
A_p	area subtended by solid angle $d\Omega$ at distance s
a	distance from center of orifice to differential area of orifice
D	diameter of cylindrical tube
$d\dot{n}$	differential molecular flow rate
d_m	cesium molecular diameter, 5.4×10^{-8} cm
f	fraction of molecules diffusely reflected from wall of tube, eq. (13)
$I(\theta)$	ion current measured by cesium probe at angle θ from tube axis
K	Knudsen number, ratio of mean free path to diameter of flow tube, $\bar{\lambda}/D$
K_a	Clausing factor
k	Boltzmann constant
L	length of cylindrical tube
m	mass of gas particle
$\dot{n}$	total molecular flow rate, molecules/sec
P	pressure in vaporizer
ΔP	average pressure drop across cylindrical tube
R	distance of test point or probe from center of orifice
r	radius of orifice
s	distance from dA_H to point (R,θ)
T	temperature of vaporizer, ^{o}K
$T(\theta)$	function of angle θ ranging in value from 1 to less than 1
$\bar{v}$	average molecular speed in vaporizer
x	ratio of a/R

z empirical coefficient, eq. (9)

α angular position of differential area, in plane of orifice, with respect to center of orifice

θ angular position of test point or probe from tube axis with respect to end of tube, also flow direction angle measured from normal to flow area

λ molecular mean free path

$\bar{\lambda}$ average molecular mean free path

μ coefficient of viscosity

$\bar{\rho}$ average density of gas, $\bar{\rho} = m\bar{\sigma}$

σ number density

Ω solid angle

APPENDIX B

DERIVATION OF KNUDSEN'S EQUATION FOR NEAR FIELD FOR THIN CIRCULAR ORIFICE

The number of particles per second leaving a differential area dA_H in the orifice that are intercepted by a sampling area A_p located at (R,θ) is given by

$$\dot{dn}_p = \frac{\Omega_1}{4\pi} \bar{\sigma v} \cos \theta' \, dA_H \tag{B1}$$

where θ' is the angle between s and the normal to dA_H. The solid angle Ω_1 encompasses the particles flowing from dA_H that are intercepted by the sampling area $A_p (A_p \ll A_H)$. The sampling area A_p is normal to R, so that

$$\Omega_1 = \frac{A_p}{s^2} \cos \theta'' \tag{B2}$$

where θ'' is the angle between s and R. With these definitions and noting that $dA_H = a \, da \, d\alpha$, equation (B1) takes the form

$$\dot{dn}_p = \frac{A_p}{4\pi} \frac{\bar{\sigma v}}{s^2} \cos \theta' \cos \theta'' \, a \, da \, d\alpha \tag{B3}$$

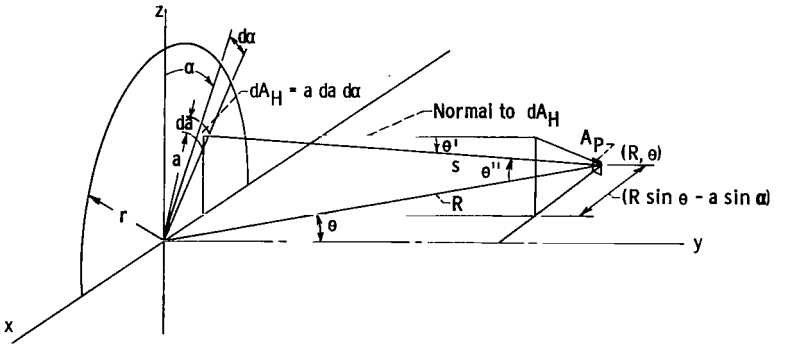

(c)

From inspection of sketch (c) it can be seen that the following relations hold:

$$\cos \theta' = \frac{R \cos \theta}{s} \tag{B4}$$

$$\cos \theta'' = \frac{R^2 + s^2 - a^2}{2Rs} \tag{B5}$$

$$s^2 = R^2 + a^2 - 2aR \sin \theta \sin \alpha \tag{B6}$$

Substituting equations (B4) to (B6) into equation (B3) yields

$$\dot{dn}_p = \frac{A_p}{4\pi} \frac{\bar{\sigma v} aR \cos \theta (R - a \sin \theta \sin \alpha) da \, d\alpha}{(R^2 + a^2 - 2Ra \sin \theta \sin \alpha)^2} \tag{B7}$$

If x, a dimensionless quantity, is defined as $x = a/R$, equation (B7) becomes

$$d\dot{n}_p = \frac{A_p}{4\pi} \frac{\bar{\sigma v} x \cos\theta (1 - x \sin\theta \sin\alpha) dx\, d\alpha}{(1 + x^2 - 2x \sin\theta \sin\alpha)^2} \tag{B8}$$

and integrating over the area A_H of the circular orifice yields the directed flow from the orifice:

$$\dot{n}_p(\theta) = \frac{A_p \bar{\sigma v} \cos\theta}{2\pi} \int_{\pi/2}^{3\pi/2} \int_0^{r/R} \frac{(1 - x \sin\theta \sin\alpha) x\, dx\, d\alpha}{(1 + x^2 - 2x \sin\theta \sin\alpha)^2} \tag{B9}$$

Carrying out the integration on x yields

$$\dot{n}_p(\theta) = \frac{A_p \bar{\sigma v}}{4\pi} \cos\theta \left(\frac{r}{R}\right)^2 \int_{\pi/2}^{3\pi/2} \frac{d\alpha}{1 + \left(\frac{r}{R}\right)^2 - 2 \frac{r}{R} \sin\theta \sin\alpha} \tag{B10}$$

which is the desired equation (3) in the text.

REFERENCES

1. Dayton, B. B.: Gas Flow Patterns at Entrance and Exit of Cylindrical Tubes. Comm. on Vacuum Techniques, 1956 Vacuum Symposium Trans., p. 5-11.

2. Clausing, P.: The Flowing of Very Dilute Gases Through Tubes of Any Length. Ann. Physik, vol. 12, 1932, pp. 961-989.

3. Sparrow, E. M., Jonsson, V. K., and Lundgren, T. S.: Free-Molecule Tube Flow and Adiabatic Wall Temperatures. Jour. Heat Transfer (Trans. ASME), ser. C, vol. 85, no. 2, May 1963, pp. 111-118; discussion, p. 118. (See also Paper 62-HT-35, ASME, 1962.)

4. Emmons, H. W., ed.: Fundamentals of Gas Dynamics. John Wiley & Sons, Inc., 1956.

5. Knudsen, M. H. C.: The Kinetic Theory of Gases. Third ed., John Wiley & Sons, Inc., 1950.

6. Dushman, S.: Scientific Foundations of Vacuum Technique. John Wiley & Sons, Inc., 1958.

7. Present, R. D.: Kinetic Theory of Gases. McGraw Hill Book Co., Inc., 1958.

8. Kennard, E. H.: Kinetic Theory of Gases. McGraw Hill Book Co., Inc., 1938.

9. Taylor, John Bradshaw, and Langmuir, Irving: The Evaporation of Atoms, Ions, and Electrons from Cesium Films on Tungsten. Phys. Rev., vol. 44, no. 6, Sept. 15, 1933, pp. 423-458.

10. Taylor, John Bradshaw, and Langmuir, Irving: Vapor Pressure of Caesium by the Positive Ion Method. Phys. Rev., vol. 51, May 1937, pp. 753-760.

TABLE I. - TABULATION OF DATA FOR KNUDSEN NUMBER OF 9.5 AND LENGTH TO DIAMETER RATIO OF 0.024

Probe position, θ, deg	Probe at 2.45 in.			Probe at 3.45 in.		
	Ion current, amp	Corrected current, amp	$\frac{\text{Current at } \theta}{\text{Current at } \theta = 0}$	Ion current, amp	Corrected current, amp	$\frac{\text{Current at } \theta}{\text{Current at } \theta = 0}$
0	87.5×10^{-9}	86.7×10^{-9}	1.0	44×10^{-9}	42.6×10^{-9}	1.0
5	87.0	86.2	.99	43.5	42.1	.99
10	86	85.2	.98	42.5	41.1	.96
15	83.5	82.7	.95	41.5	40.1	.94
20	82	81.2	.94	40	38.6	.91
25	79	78.2	.90	39	37.6	.88
30	76.5	75.7	.87	38	36.6	.86
35	73	72.2	.83	35	33.6	.79
40	68	67.2	.78	32.5	31.1	.73
45	61.5	60.7	.70	30.5	29.1	.68
50	56	55.2	.64	28	26.6	.62
55	50	49.2	.57	24	22.6	.53
60	44	43.2	.50	22	20.6	.48
65	37	36.2	.42	18	16.6	.40
70	33	32.2	.37	14	12.6	.30
75	23.5	22.7	.26	11	9.6	.23
80	16	15.2	.18	7.25	5.85	.14
85	11.5	10.7	.12	4	2.6	.06
90	.8	0	0	1.4	0	0

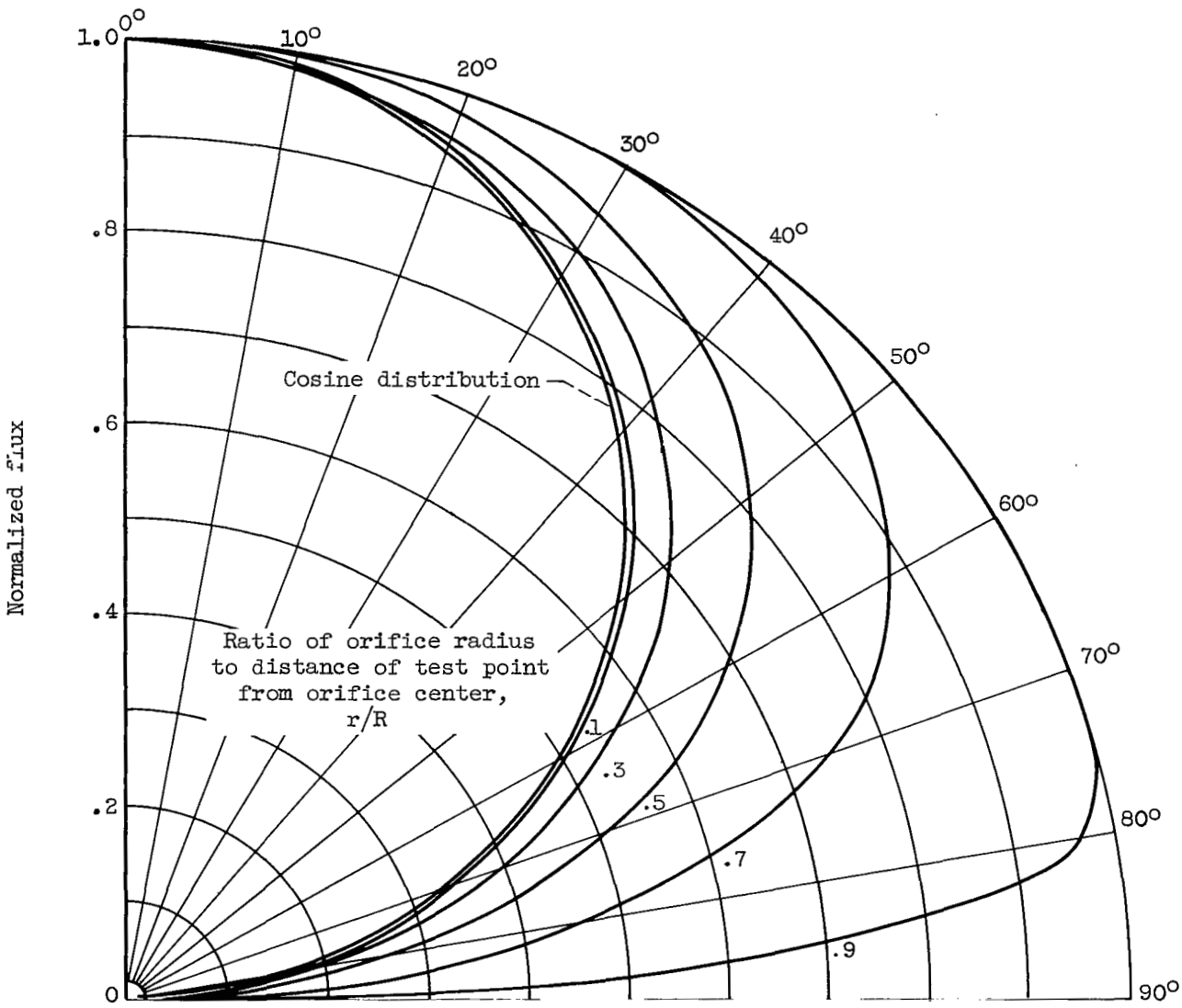

Figure 1. - Plot of efflux pattern from thin orifice for various values of ratio of orifice radius to distance of test point from orifice center.

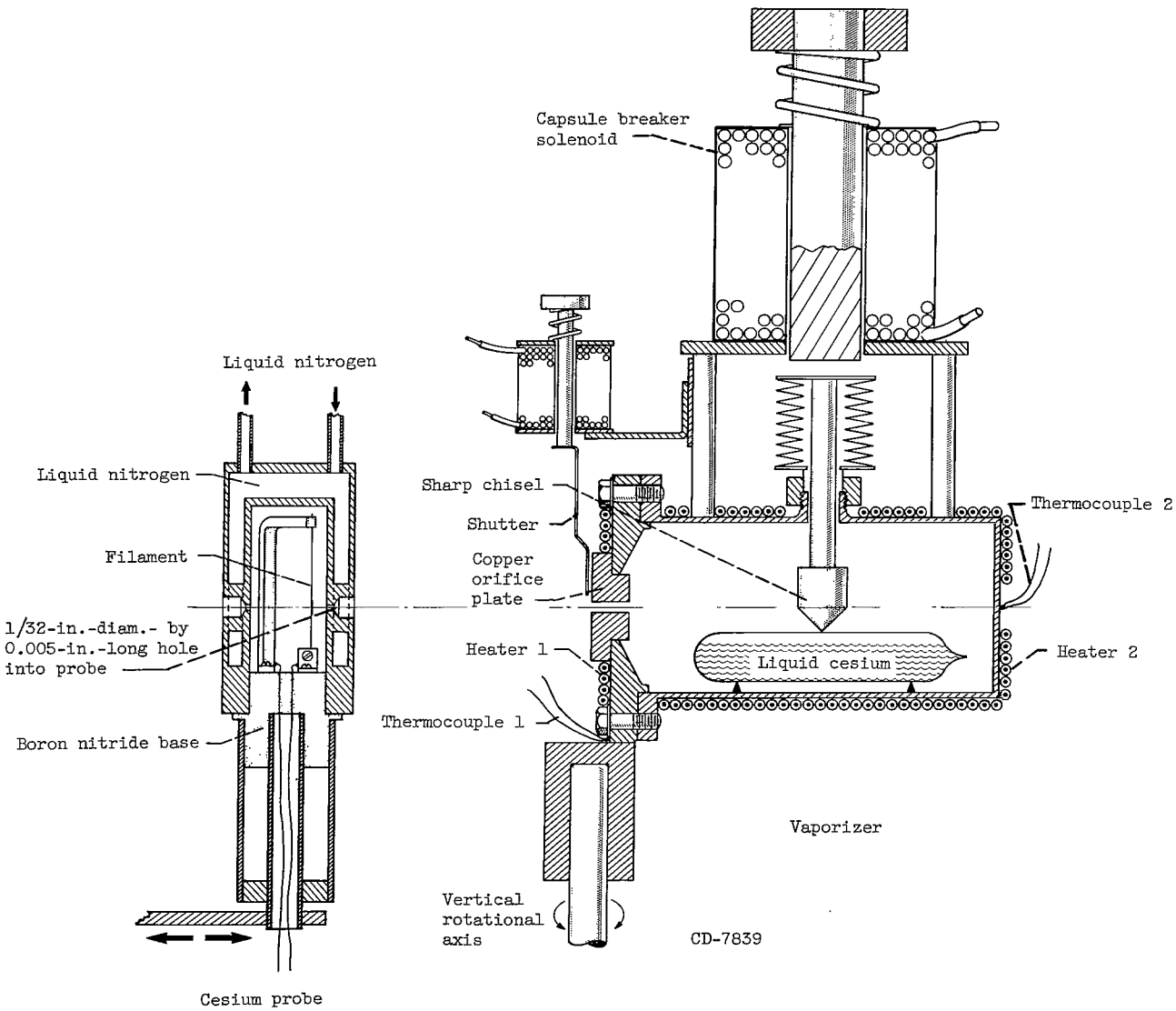

(a) Schematic drawing.

Figure 2. - Vaporizer used to measure efflux patterns.

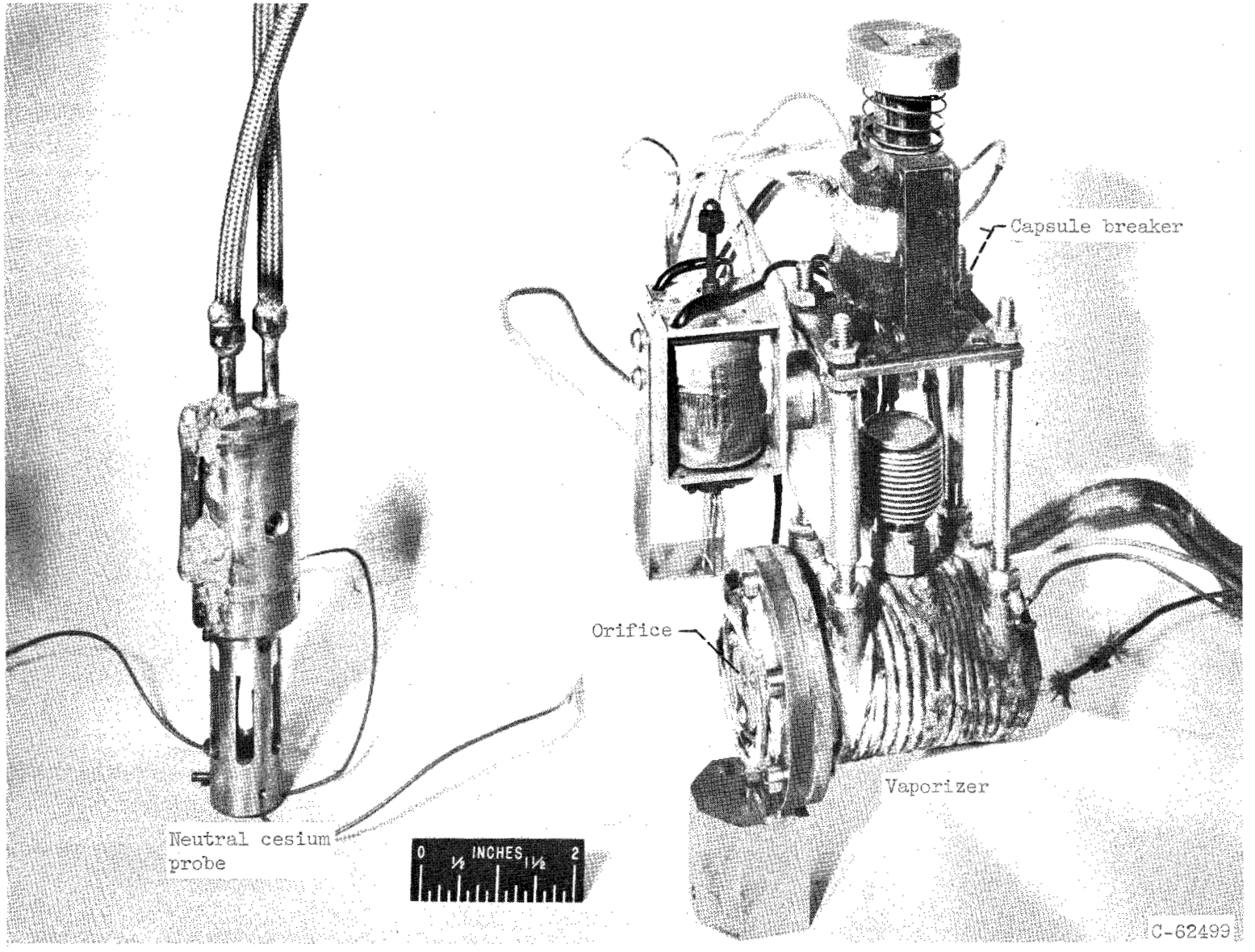

(b) Photograph.

Figure 2. - Concluded. Neutral cesium probe and vaporizer used to measure efflux patterns.

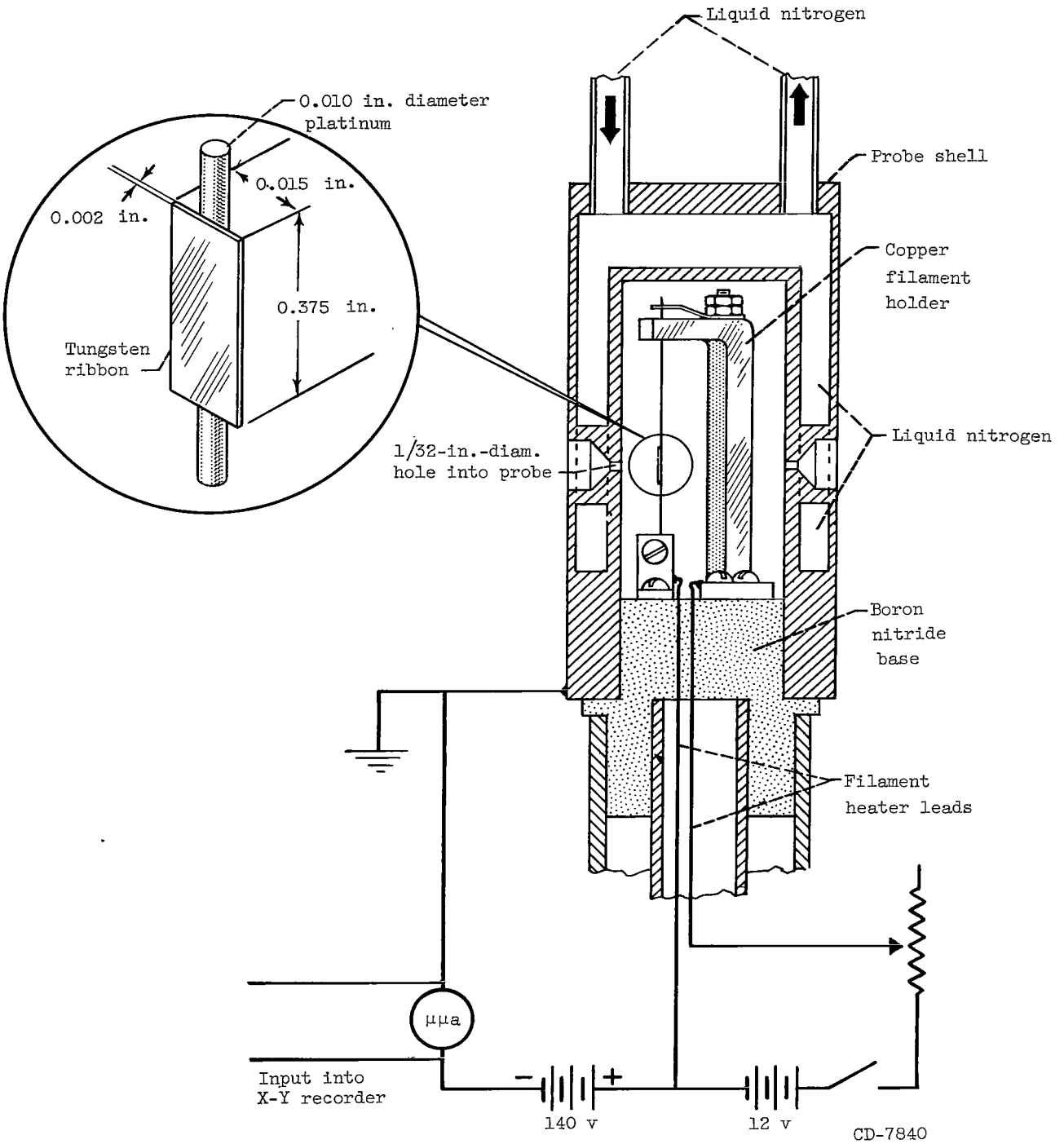

Figure 3. - Cesium probe and electrical circuit.

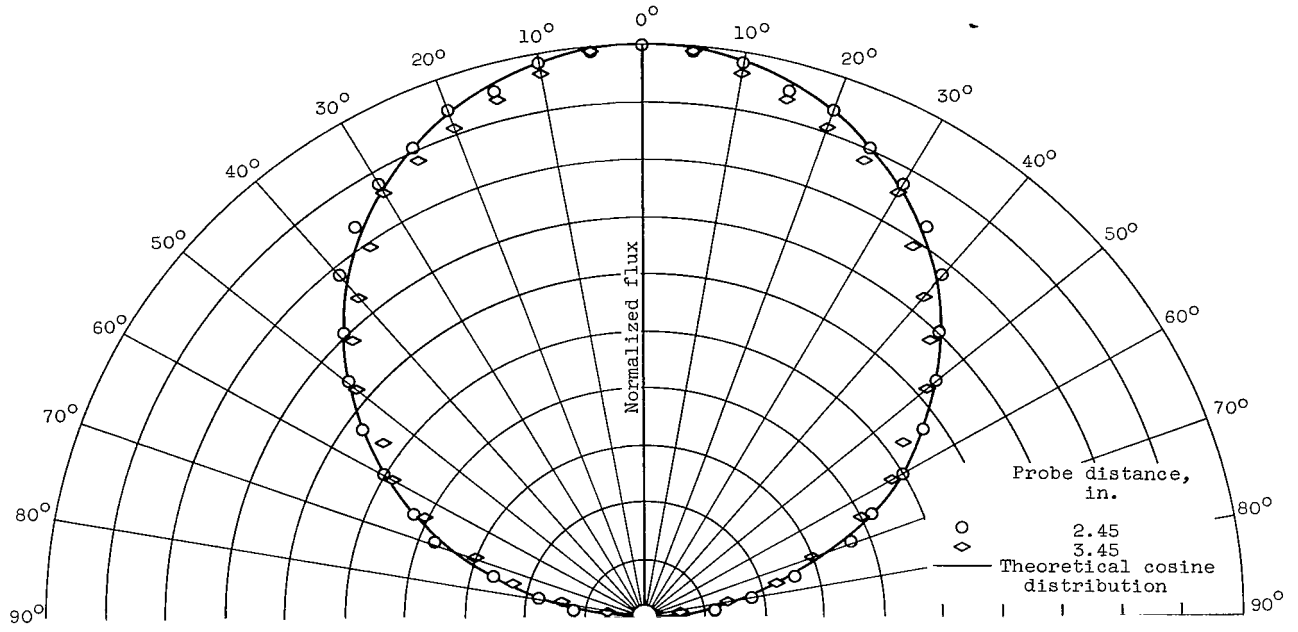

Figure 4. - Efflux pattern for free-molecule flow (Knudsen number, 9.5) from thin circular orifice with length to diameter ratio of 0.024.

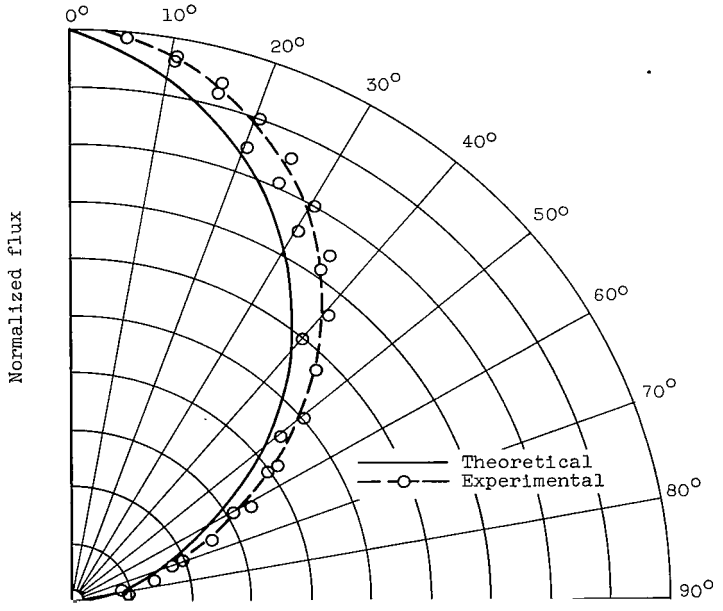

(a) Length to diameter ratio, 0.5.

Figure 5. - Efflux pattern of cesium vapor from cylindrical tube for free-molecule flow; at various length to diameter ratios. Knudsen number, 9.5.

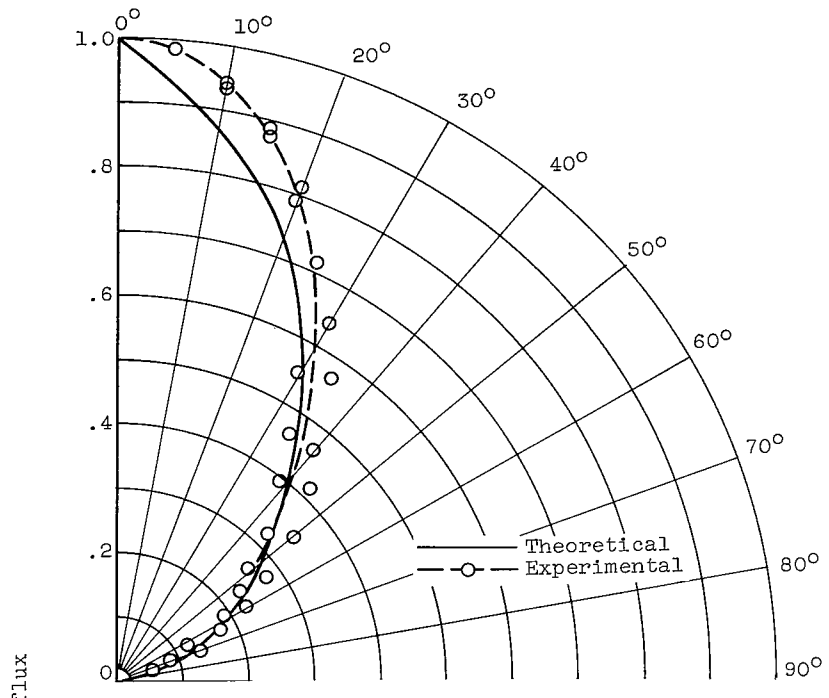

(b) Length to diameter ratio, 1.

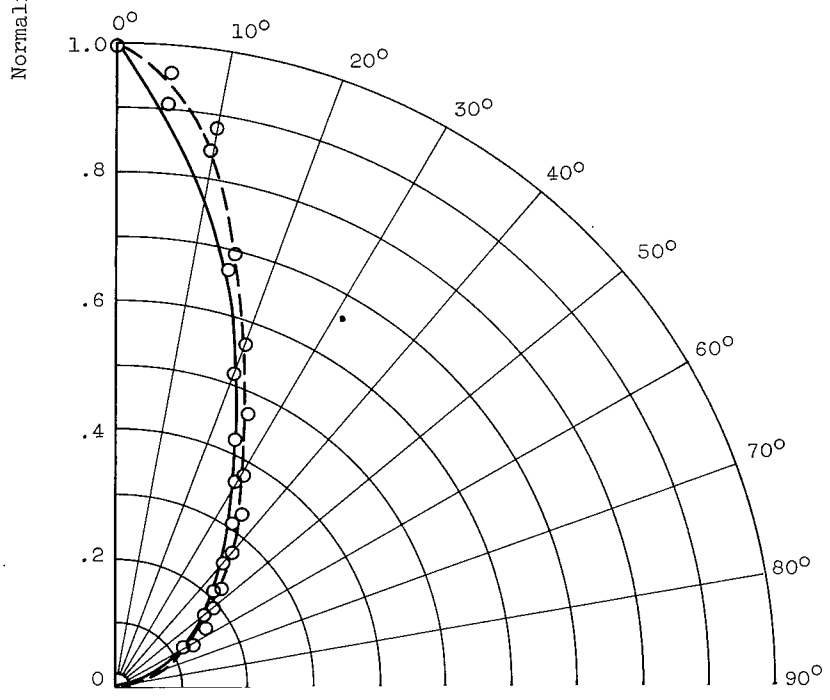

(c) Length to diameter ratio, 2.

Figure 5. - Continued. Efflux pattern of cesium vapor from cylindrical tube for free-molecule flow at various length to diameter ratios. Knudsen number, 9.5.

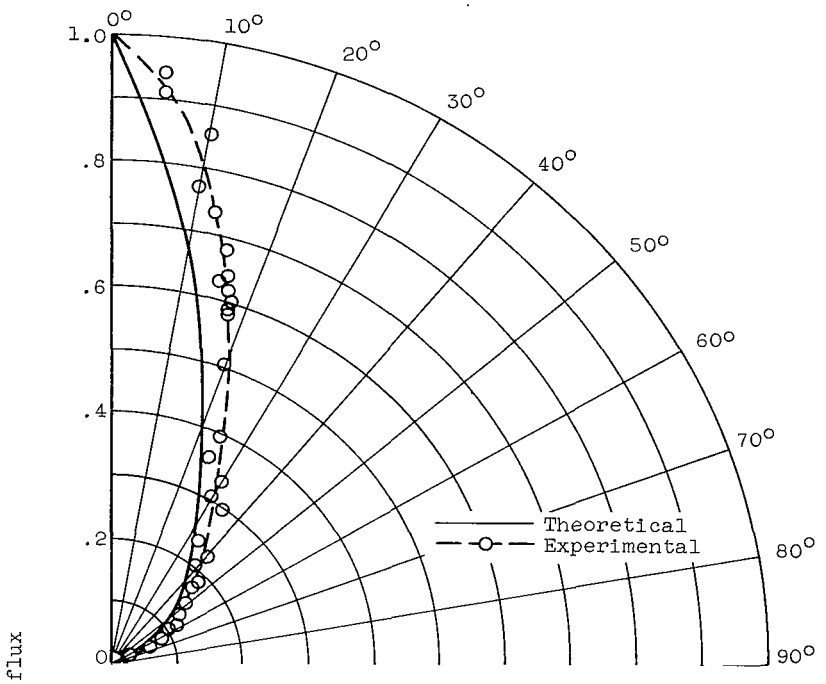

(d) Length to diameter ratio, 3.

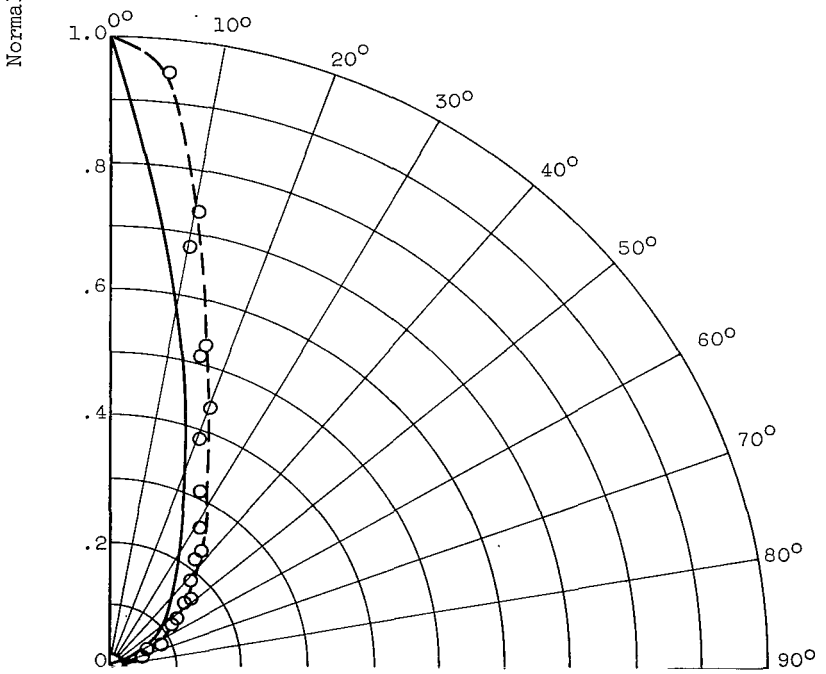

(e) Length to diameter ratio, 4.

Figure 5. - Concluded. Efflux pattern of cesium vapor from cylindrical tube for free-molecule flow at various length to diameter ratios. Knudsen number, 9.5.

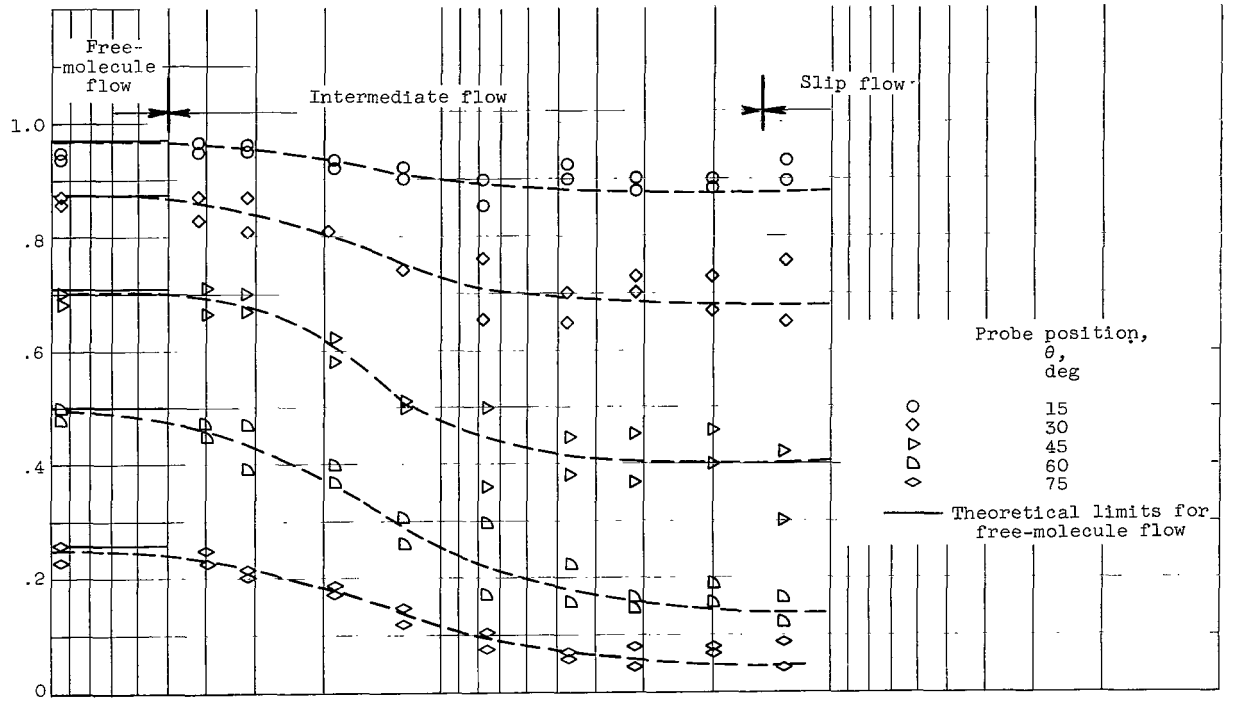

(a) Length to diameter ratio, 0.024.

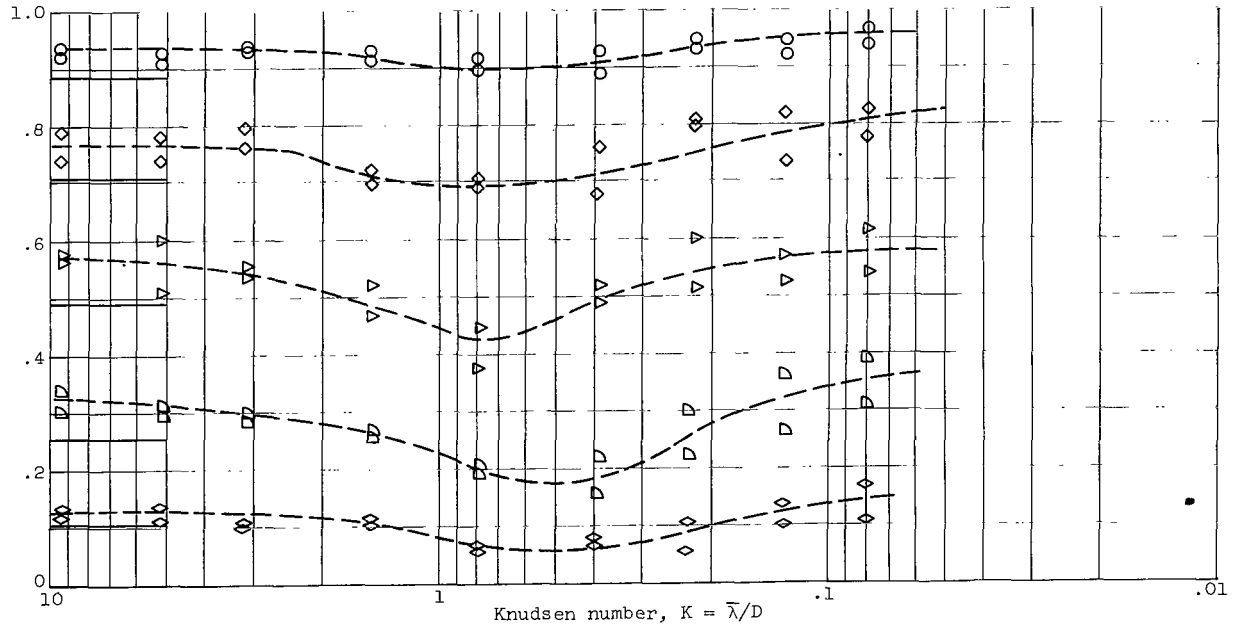

(b) Length to diameter ratio, 0.5.

Figure 6. - Experimental values of $T(\theta)\cos\theta$ for cesium vapor for specific values of probe position over a range of Knudsen number at various length to diameter ratios.

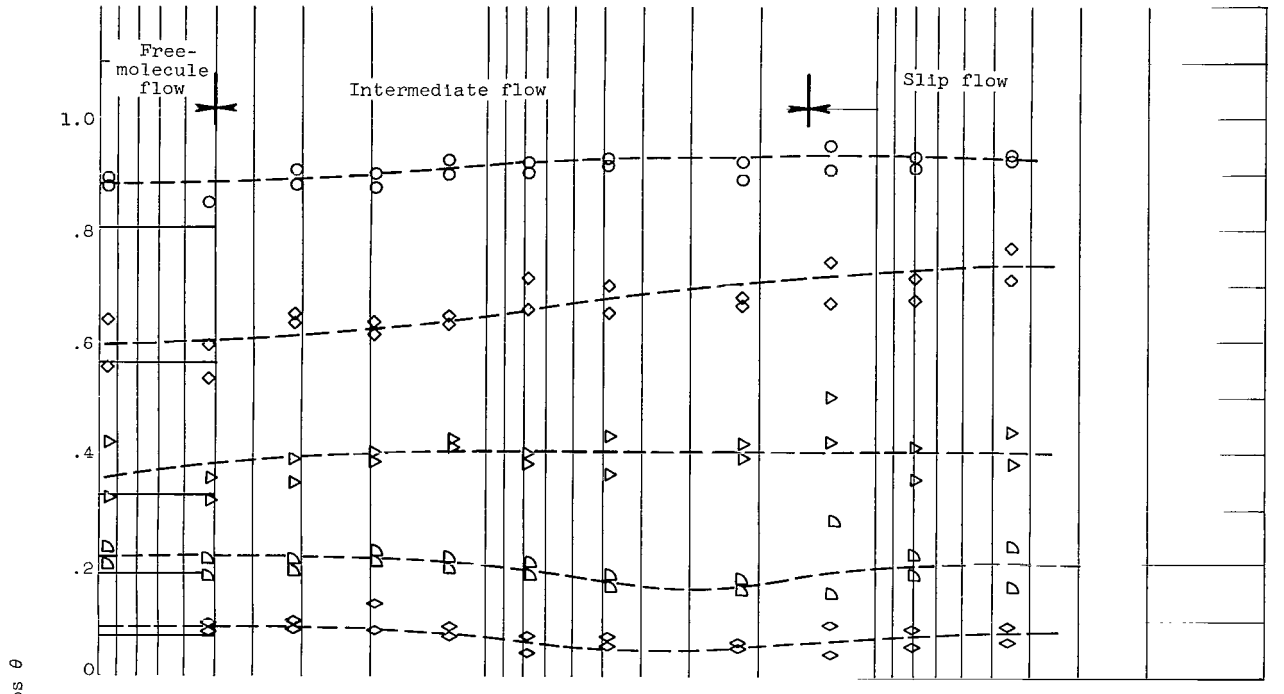

(c) Length to diameter ratio, 1.

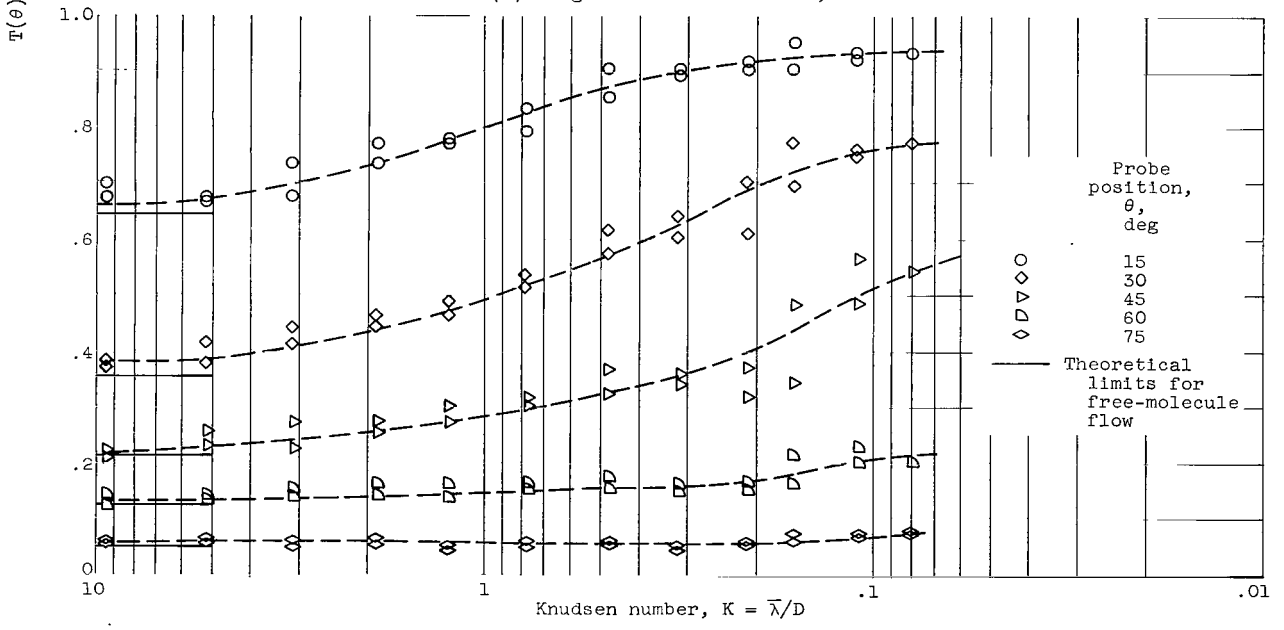

(d) Length to diameter ratio, 2.

Figure 6. - Continued. Experimental values of $T(\theta)\cos\theta$ for cesium vapor for specific values of probe position over a range of Knudsen number at various length to diameter ratios.

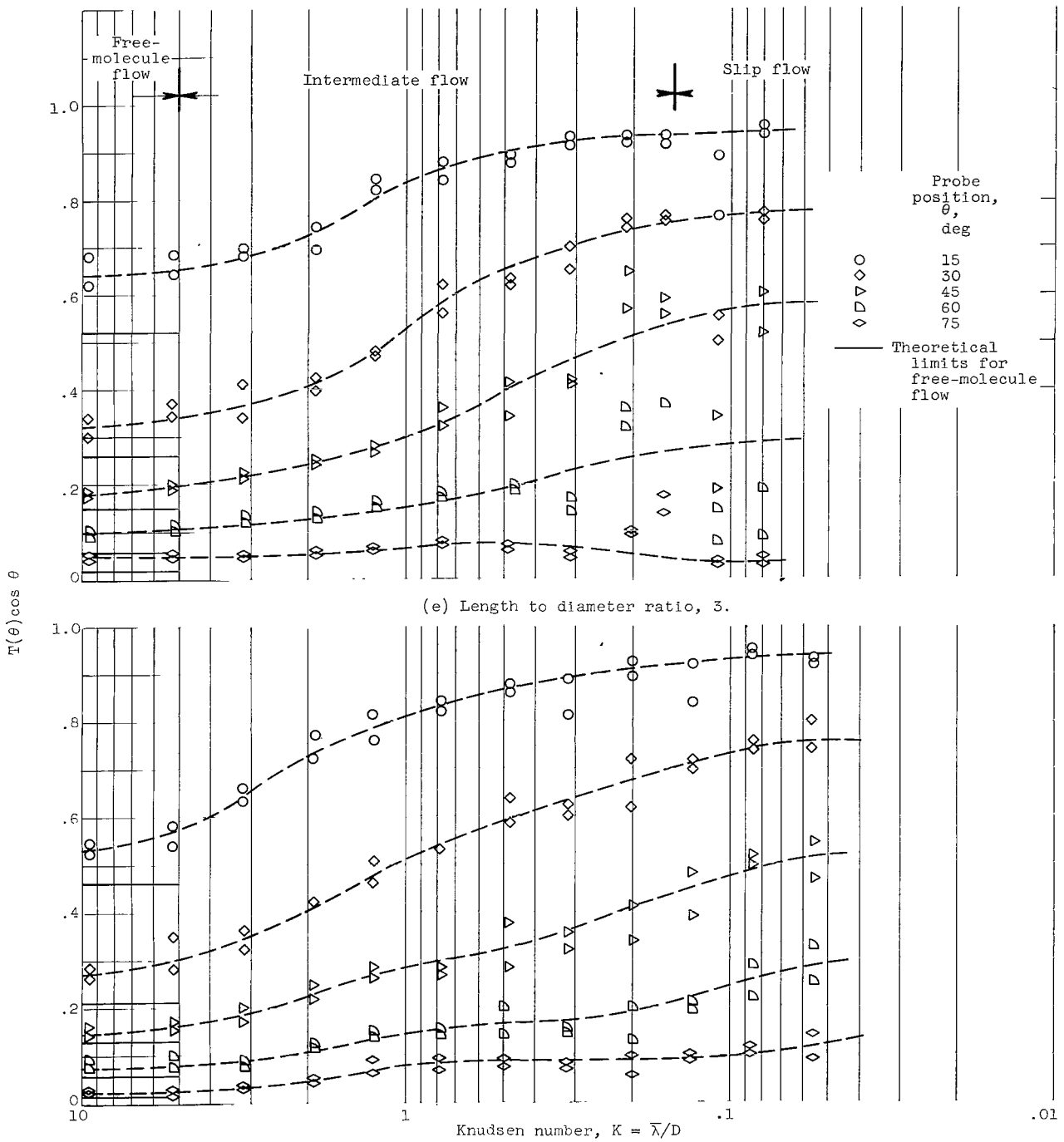

(e) Length to diameter ratio, 3.

(f) Length to diameter ratio, 4.

Figure 6. - Concluded. Experimental values of $T(\theta)\cos\theta$ for cesium vapor for specific values of probe position over a range of Knudsen number at various length to diameter ratios.

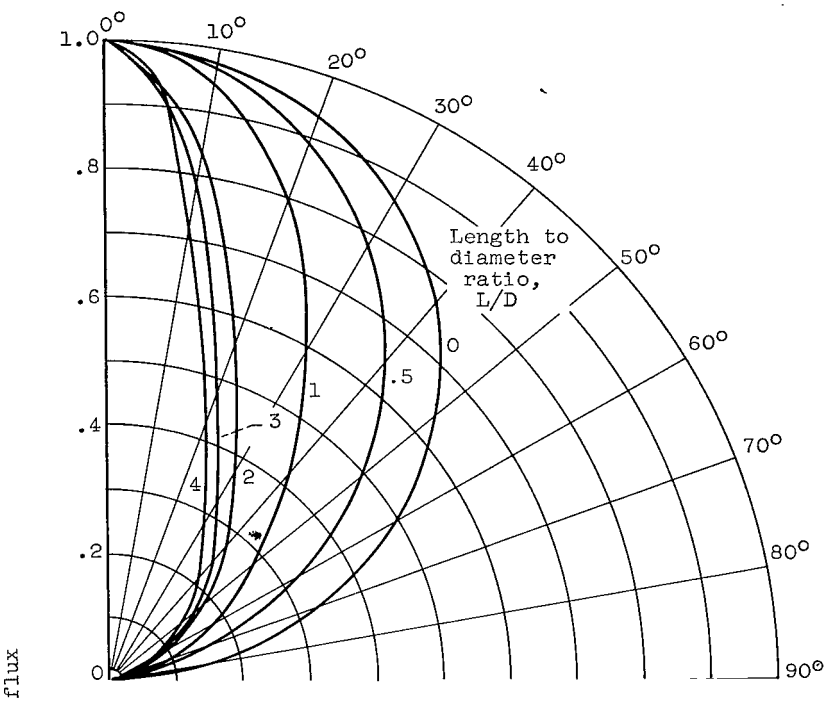

(a) Free-molecule-flow regime; Knudsen number, 9.5.

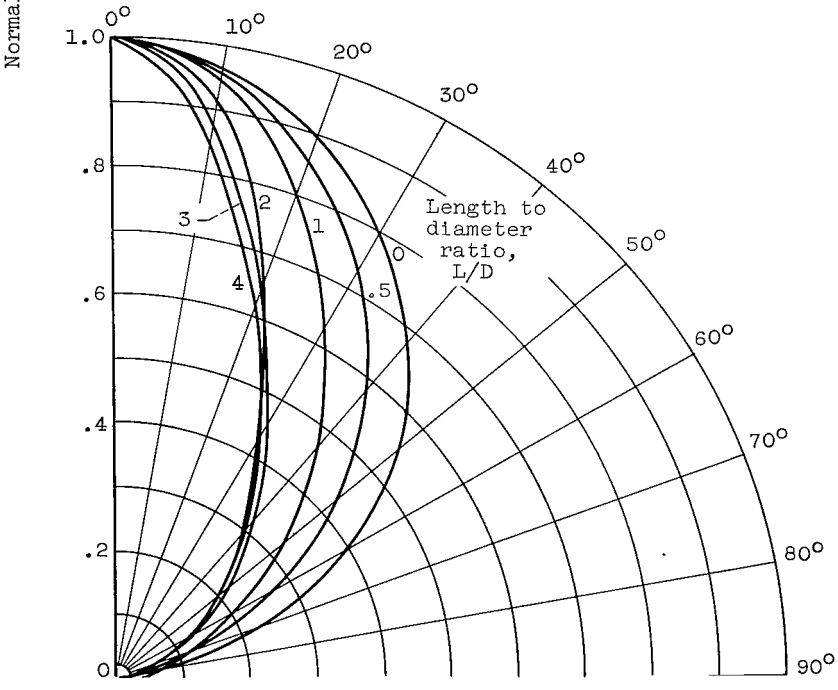

(b) Intermediate-flow regime; Knudsen number, ~1.9.

Figure 7. - Experimental efflux patterns of cesium vapor from cylindrical tubes of various length to diameter ratios.

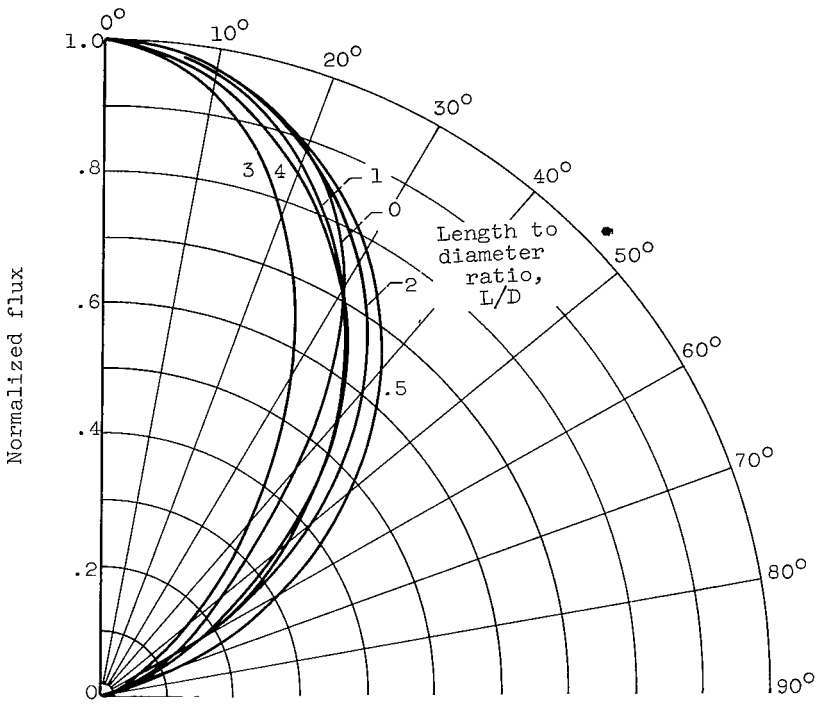

(c) Slip-flow regime; Knudsen number, 0.12.

Figure 7. - Concluded. Experimental efflux patterns of cesium vapor from cylindrical tubes of various length to diameter ratios.

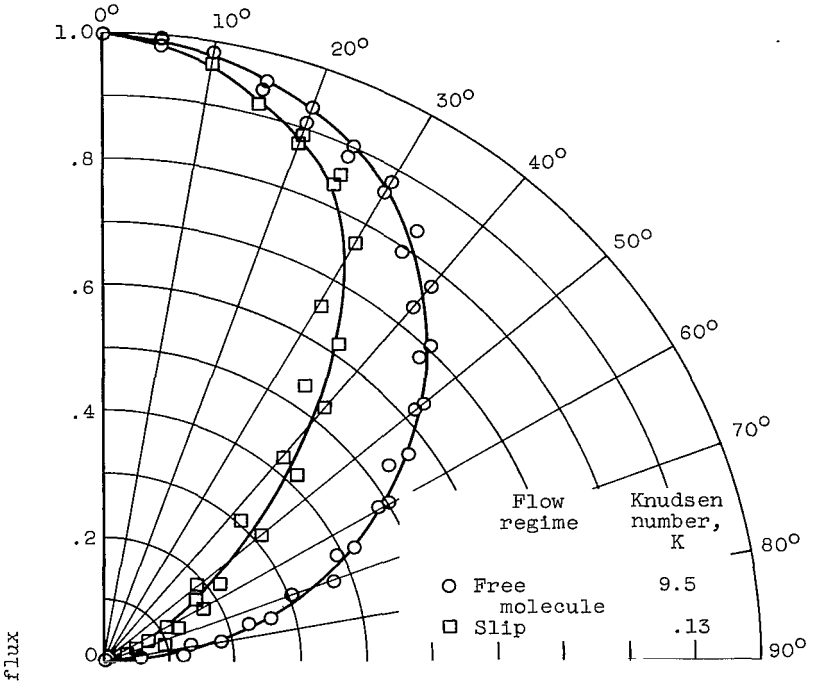

(a) Length to diameter ratio, 0.024.

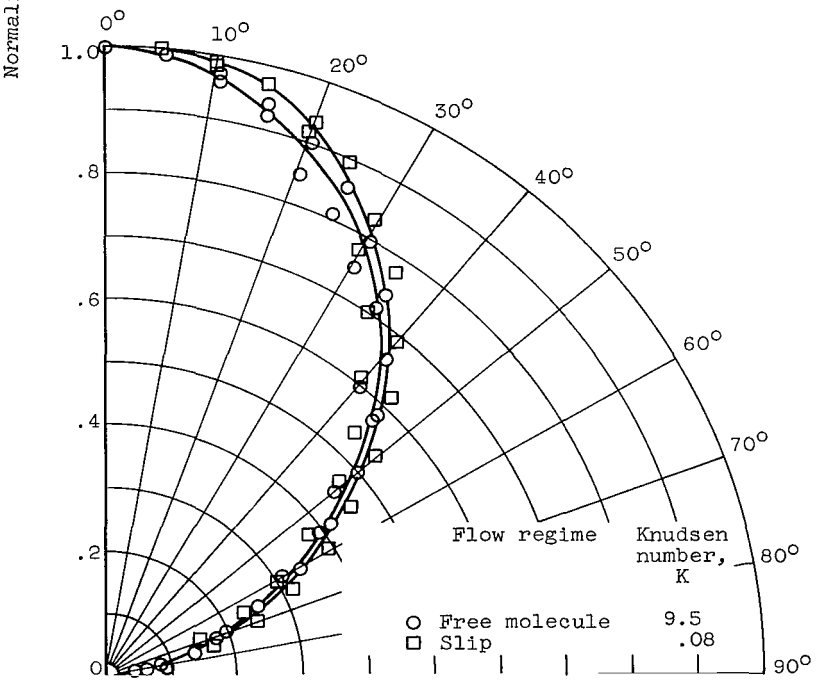

(b) Length to diameter ratio, 0.5.

Figure 8. - Experimental efflux pattern of cesium vapor from a cylindrical tube for free-molecule and slip flows.

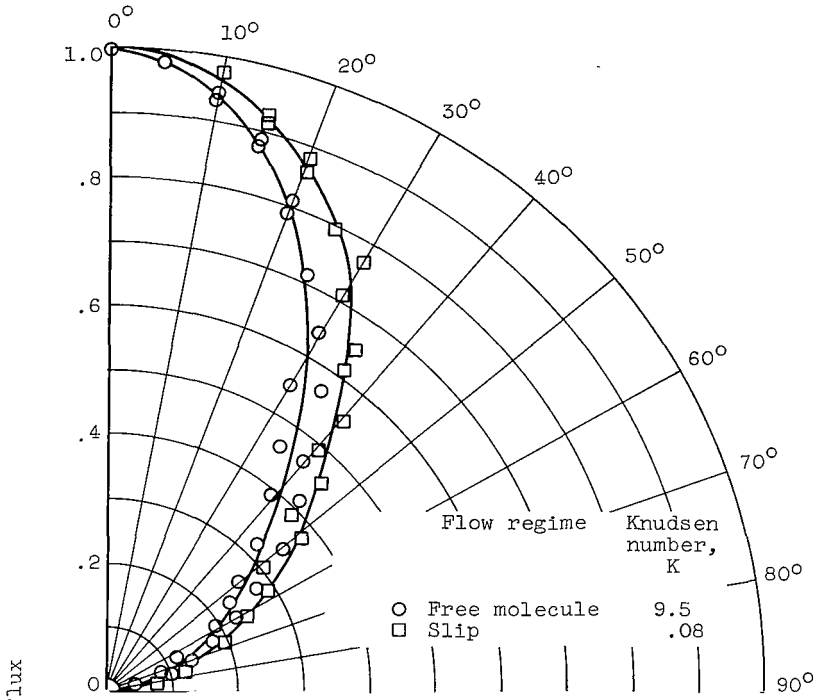

(c) Length to diameter ratio, 1.

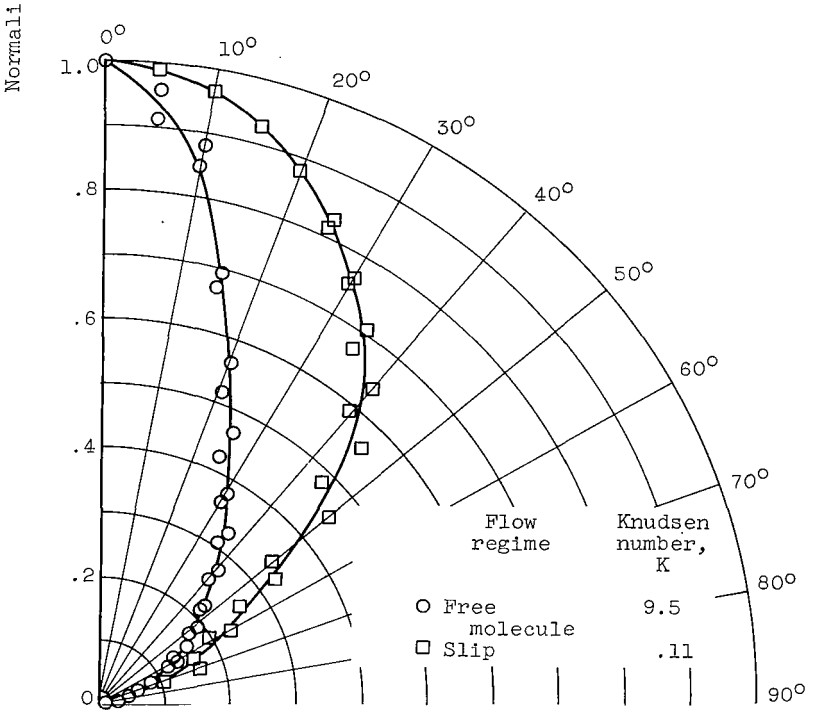

(d) Length to diameter ratio, 2.

Normalized flux

Figure 8. - Continued. Experimental efflux pattern of cesium vapor from cylindrical tube for free-molecule and slip flows.

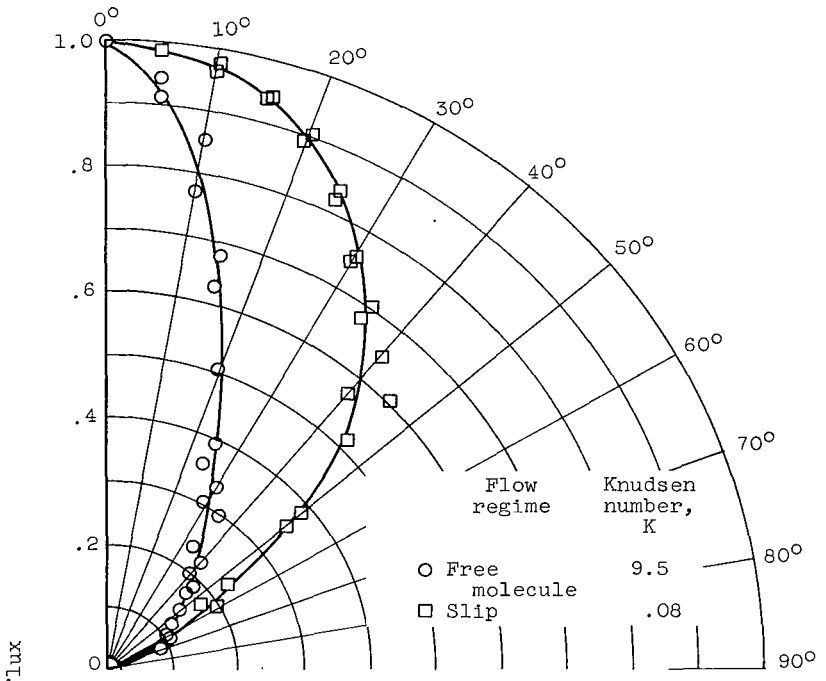

(e) Length to diameter ratio, 3.

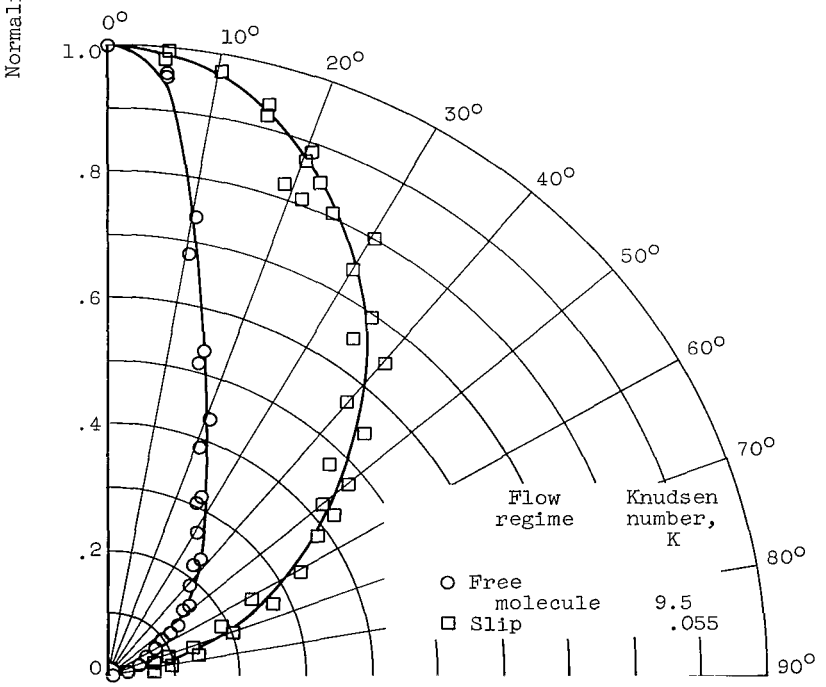

(f) Length to diameter ratio, 4.

Normalized flux

Figure 8. - Concluded. Experimental efflux pattern of cesium vapor from cylindrical tube for free-molecule and slip flows.

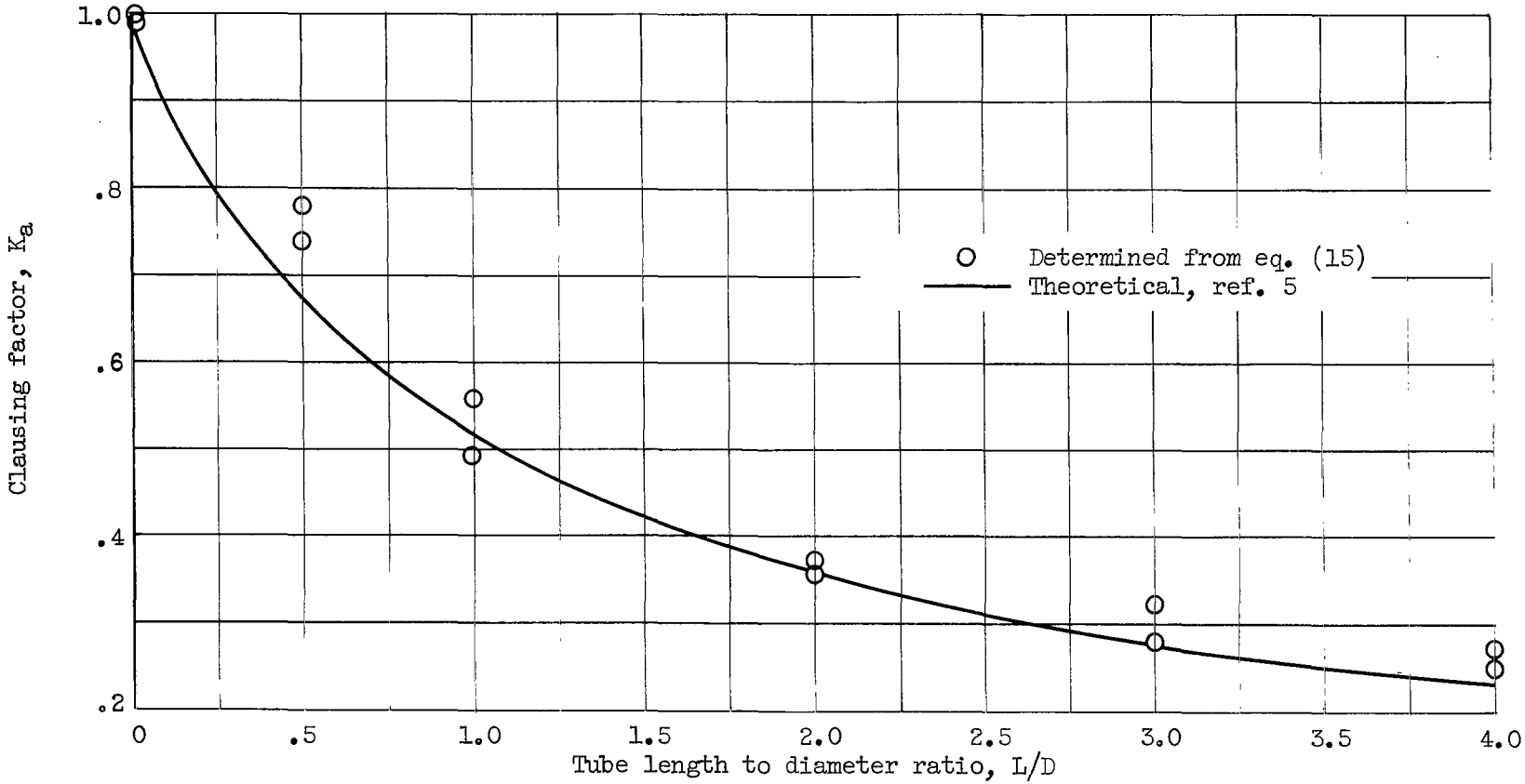

Figure 9. - Variation of Clausing factor with tube length to diameter ratio for Knudsen number of 9.5.

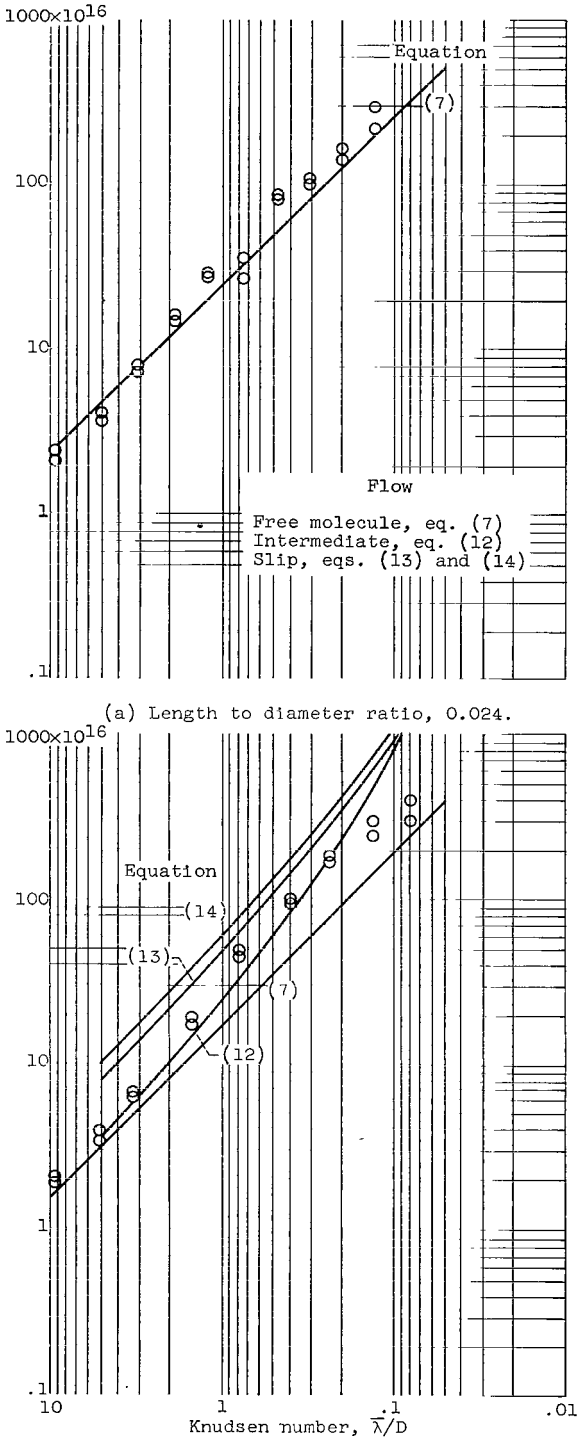

Figure 10. - Variation of flow rate with Knudsen number for tubes of various length to diameter ratios. Tube diameter, 0.125 inch.

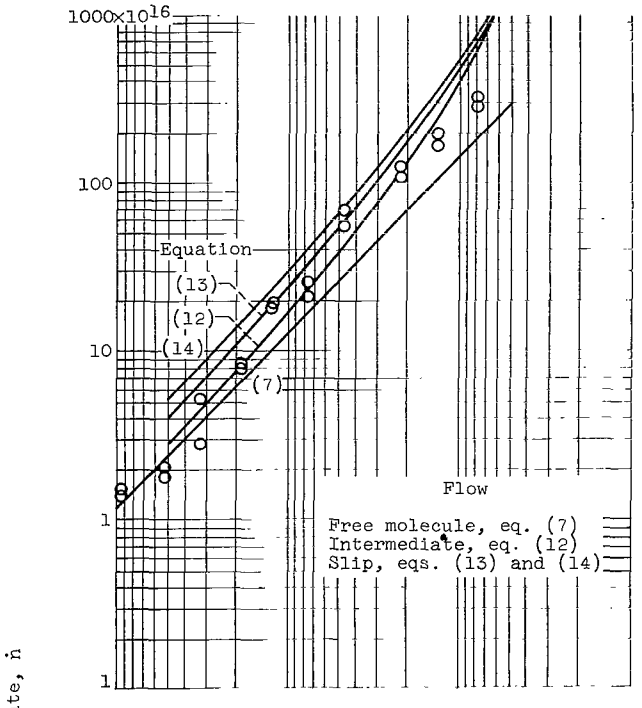

(c) Length to diameter ratio, 1.

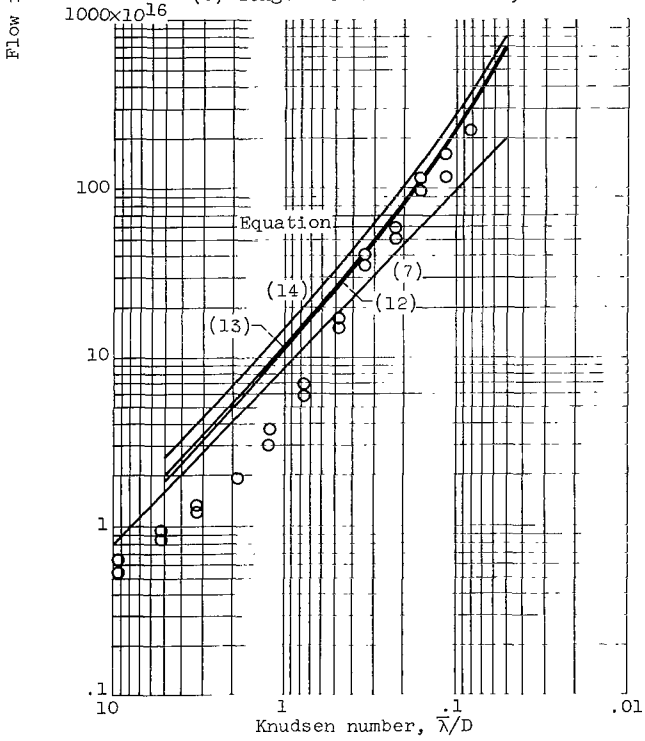

(d) Length to diameter ratio, 2.

Figure 10. - Continued. Variation of flow rate with Knudsen number for tubes of various length to diameter ratios. Tube diameter, 0.125 inch.

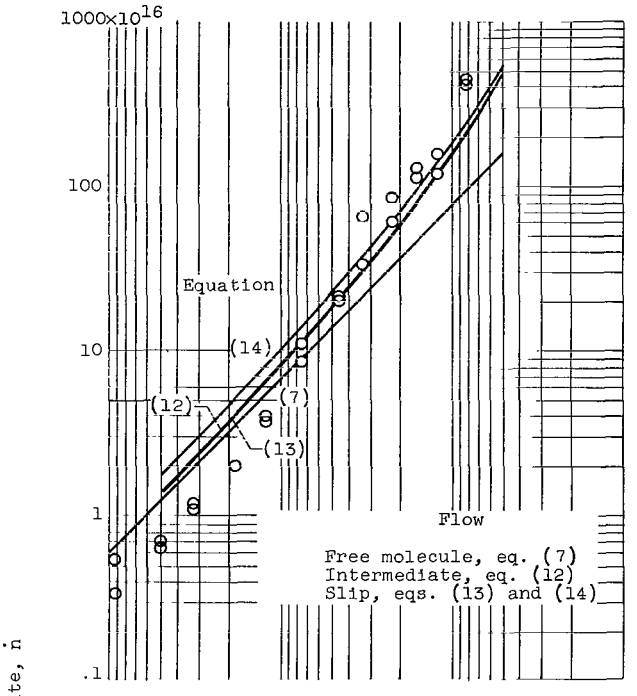

(e) Length to diameter ratio, 3.

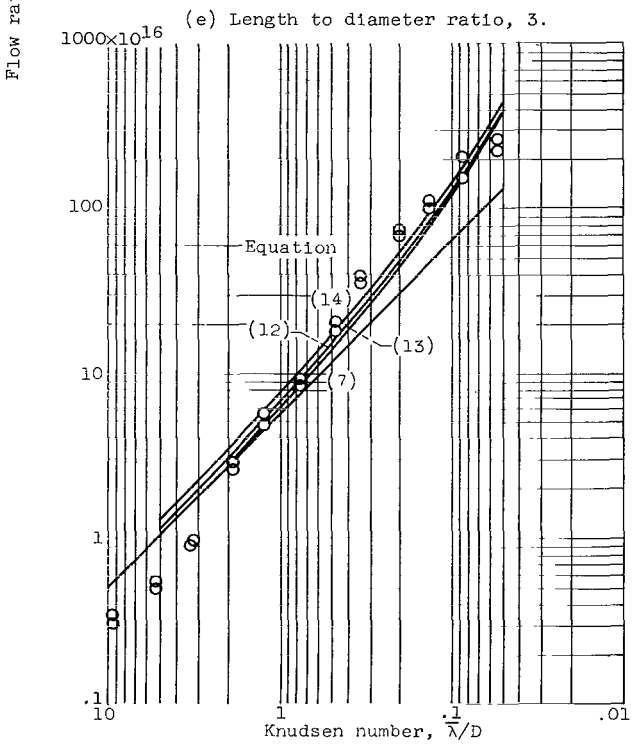

(f) Length to diameter ratio, 4.

Figure 10. - Concluded. Variation of flow rate with Knudsen number for tubes of various length to diameter ratios. Tube diameter, 0.125 inch.

"The aeronautical and space activities of the United States shall be conducted so as to contribute . . . to the expansion of human knowledge of phenomena in the atmosphere and space. The Administration shall provide for the widest practicable and appropriate dissemination of information concerning its activities and the results thereof."

—NATIONAL AERONAUTICS AND SPACE ACT OF 1958

NASA SCIENTIFIC AND TECHNICAL PUBLICATIONS

TECHNICAL REPORTS: Scientific and technical information considered important, complete, and a lasting contribution to existing knowledge.

TECHNICAL NOTES: Information less broad in scope but nevertheless of importance as a contribution to existing knowledge.

TECHNICAL MEMORANDUMS: Information receiving limited distribution because of preliminary data, security classification, or other reasons.

CONTRACTOR REPORTS: Technical information generated in connection with a NASA contract or grant and released under NASA auspices.

TECHNICAL TRANSLATIONS: Information published in a foreign language considered to merit NASA distribution in English.

TECHNICAL REPRINTS: Information derived from NASA activities and initially published in the form of journal articles.

SPECIAL PUBLICATIONS: Information derived from or of value to NASA activities but not necessarily reporting the results of individual NASA-programmed scientific efforts. Publications include conference proceedings, monographs, data compilations, handbooks, sourcebooks, and special bibliographies.

Details on the availability of these publications may be obtained from:

SCIENTIFIC AND TECHNICAL INFORMATION DIVISION

NATIONAL AERONAUTICS AND SPACE ADMINISTRATION

Washington, D.C. 20546